



D3.5 Demo 2 Vehicle demonstrator for object detection in adverse weather conditions update

| | |
|-----------------------------|--|
| Primary Author(s) | Christian Löffler Robert Bosch GmbH Carina Vogl CARIAD SE Volker Labenski AUDI AG Daniel Weihmayr THI |
| Related Work Package | WP3 |
| Version/Status | 1.1 Final Version |
| Issue date | 14/10/22 |
| Deliverable type | Demonstrator |
| Dissemination Level | PU |
| Project Acronym | SAFE-UP |
| Project Title | proactive SAFETy systems and tools for a constantly UPgrading road environment |
| Project Website | www.safeup.eu |
| Project Coordinator | Núria Parera Applus IDIADA |
| Grant Agreement No. | 861570 |



This project has received funding from the European Union's Horizon 2020 research and innovation programme under Grant Agreement 861570.

Co-Authors

| Name | Organisation |
|------------------------|-------------------|
| Timm Gloger | Robert Bosch GmbH |
| Till Schwaderer | Robert Bosch GmbH |
| Markus Firmbach | Robert Bosch GmbH |
| Johann Stoll | CARIAD SE |
| Kristin Blum | CARIAD SE |
| Markus Koebe | AUDI AG |

Document Distribution

| Version | Date | Distributed to |
|---------|------------|-----------------------------|
| 1.1 | 13/10/22 | Coordination Team |
| 1.1 | 14/10/22 | Submission in the EC System |
| 1.1 | 06/03/2023 | Approved by the EC |



Copyright statement

The work described in this document has been conducted within the SAFE-UP project. This document reflects only the views of the SAFE-UP Consortium. The European Union is not responsible for any use that may be made of the information it contains.

This document and its content are the property of the SAFE-UP Consortium. All rights relevant to this document are determined by the applicable laws. Access to this document does not grant any right or license on the document or its contents. This document or its contents are not to be used or treated in any manner inconsistent with the rights or interests of the SAFE-UP Consortium or the Partners detriment and are not to be disclosed externally without prior written consent from the SAFE-UP Partners.

Each SAFE-UP Partner may use this document in conformity with the SAFE-UP Consortium Grant Agreement provisions.



Executive summary

This Deliverable falls under the SAFE-UP Project Work Package 3 “Active safety systems for vehicle-VRU interaction” and specifically under the Task 3.2 “VRU detection under bad weather conditions”. It is a purely technical document that targets to support the efficient monitoring of the technical developments for Demonstrator 2 “vehicle demonstrator for object detection in adverse weather conditions”.

The present document is the second and final of two deliverables related to Demo 2 and focuses on three additional measurement campaigns with different purposes as well as the detailed analysis and evaluation of their results. For the purpose of validating functionalities under adverse weather conditions in simulation, the weather filter which was introduced by THI in the previous report is described in its final version here as well.

The report is organized as follows: Section 2 presents an overview of the used demonstrator hardware. In section 3, the setup and conduction of the three additional measurement campaigns is described. Section 4 gives an overview about the analysis of the measurement campaigns, including their quantification of the relevant sensor degradation as well as the developed weather filter algorithm. Section 5 closes the report with a discussion, conclusion and a description of the next steps.



Table of Contents

| | |
|--|-----------|
| 1. Introduction..... | 9 |
| 2. Demonstrator hardware..... | 10 |
| 3. Measurement campaigns | 12 |
| 3.1 <i>Second measurement campaign</i> | <i>13</i> |
| 3.2 <i>Third measurement campaign</i> | <i>15</i> |
| 3.3 <i>Fourth measurement campaign</i> | <i>18</i> |
| 4. Demo 2 development | 23 |
| 4.1 <i>Overall demonstrator scope</i> | <i>23</i> |
| 4.2 <i>Results of the second measurement campaign.....</i> | <i>23</i> |
| 4.3 <i>Results of the fourth measurement campaign.....</i> | <i>40</i> |
| 4.4 <i>Weather filter</i> | <i>50</i> |
| 5. Discussion, conclusions and next steps | 58 |
| References | 59 |



List of figures

| | |
|---|----|
| Figure 1: <i>Demo 3 vehicle</i> : a Bosch development vehicle with close to series radar and video sensors. | 10 |
| Figure 2: CARIAD development vehicle featuring a 360 degrees camera belt. | 11 |
| Figure 3: Bosch development vehicle equipped with road condition and visibility (mounted on the roof top) sensors. | 11 |
| Figure 4: Bosch development vehicle with video and LiDAR sensors | 12 |
| Figure 5: General idea behind the second measurement campaign for integrating sensor models in simulations. | 13 |
| Figure 6: Investigated dummies from 4A in the second measurement campaign | 14 |
| Figure 7: Test grid of the second measurement campaign (static measurements) inside the CARISSMA test hall | 15 |
| Figure 8: Measurement setup on the example of a mirrored scenario from cluster P-CLwoSO (35kph vehicle velocity, 8kph pedestrian velocity, and a TTC of 2s) | 17 |
| Figure 9: Images of the third measurement campaign | 18 |
| Figure 10: Graphical representation of Short Range LiDAR scenario setup | 20 |
| Figure 11: Graphical representation of Long Range LiDAR scenario setup | 21 |
| Figure 12: Example histograms of the angles of the radar locations for position 1 and 3 (pedestrian, no rain, desired angle: 16°). At both positions, the nearest local maximum is at an angle of 18° instead of the originally planned 16°. | 25 |
| Figure 13: FoV in polar and Cartesian coordinates for 10sqm and nominal conditions (Robert Bosch GmbH, 2022) | 26 |
| Figure 14: Location of the used bounding box for the pedestrian target at two positions when the angle is not corrected (first row) and when the angle is corrected (second row). | 27 |
| Figure 15: Detection decision for two example positions of the pedestrian target at a rain intensity of 16mm/h. | 28 |
| Figure 16: Grid of detected and not detected positions for the pedestrian target for dry conditions. | 29 |



Figure 17: Measurement points with fitted FoVs for the radar sensor, the pedestrian target and different weather settings 30

Figure 18: Visualization of the two different camera modes..... 31

Figure 19: Visualization of assumed effects on the detectability (left) and the chosen interpolation points (right)..... 32

Figure 20: Fitted polynomial function in polar coordinates and transformation to the vehicle coordinate system. 33

Figure 21: Grid of detected and not detected positions for the pedestrian target for dry conditions..... 34

Figure 22: Measured points and corresponding camera detections for the pedestrian target under rainy conditions with fitted theoretical FoVs. 35

Figure 23: Summary of the results for the investigated radar (top) and video (bottom) sensor at dry and rainy conditions in Cartesian coordinates (left) and polar coordinates (right) 36

Figure 24: Crossing from left without sight obstruction (CLwoSO) – Trajectories, relative and Radar FoV for different rain levels 39

Figure 25: Target visibility 41

Figure 26: Detection probability 42

Figure 27: Intensity analysis for a rain environment 43

Figure 28: Detection probability analysis for a rain environment 43

Figure 29: Intensity analysis for a fog environment 44

Figure 30: Detection probability analysis for a fog environment 45

Figure 31: Effects of the wiper cleaning system 46

Figure 32: Comparison of the measured visibility range of two fog sensors. The result of the stationary device Sick Visic620 is shown as blue curve. For the mobile sensor mounted on the vehicle Campbell CS125 the result is shown in orange. 48

Figure 33: Comparison of results of the road condition sensor and images during measurement campaign. The panels show (a) the surface state, (b) water layer thickness and (e) visibility range. 50

Figure 34: Weather filter implementation within the given software framework..... 51



Figure 35: Dependency between fog density and visible range (SAFE-UP, Deliverable report D2.10, 2022) 52

Figure 36: Lidar attenuation dependency on rain and fog (SAFE-UP, Deliverable report D2.10, 2022)..... 52

Figure 37: Radar attenuation dependency on rain and fog (SAFE-UP, Deliverable report D2.10, 2022)..... 53

Figure 38: Camera attenuation for different rain conditions (SAFE-UP, Deliverable report D2.10, 2022)..... 54

Figure 39: Detection thresholds per target class for radar under rain (SAFE-UP, Deliverable report D2.10, 2022) 54

Figure 40: Detection thresholds per target class for radar under fog..... 55

Figure 41: Detection thresholds per target class for lidar under rain 55

Figure 42: Detection thresholds per target class for lidar under fog 56

Figure 43: Detection thresholds per target class for camera under rain 56

Figure 44: Detection thresholds per target class for camera under fog 57

List of tables

Table 1: Summary of selected scenarios for Demo 2 with suggestions for test speeds and TTCs. 16

Table 2: Tested configurations in the third measurement campaign 17

Table 3: Target under different weather conditions 19

Table 4: Target in Fog 20

Table 5: Target in Rain..... 21

Table 6: Summary of the angles, which were corrected for the pedestrian tests in dry and rainy settings..... 25

Table 7: Comparison of the extracted values of the GIDAS to the ranges defined by the German weather service DWD for the intensity labels. Table from (SAFE-UP, Deliverable report D2.6, 2021) 37



List of abbreviations

| Abbreviation | Meaning |
|-----------------|---|
| VRU | Vulnerable Road User |
| TTC | Time-to-Collision |
| P-CLwoSO | Pedestrian crossing left without sight obstruction |
| B-CR | Cyclist crossing from right while passenger car moves forward |
| KSI | Killed or seriously injured |
| FOV | Field-Of-View |



1. Introduction

This deliverable reports on the development of WP3 Demo 2. The goal of Demo 2 is to both quantify and optimize VRU detection of active safety systems in adverse weather conditions by taking real-world scenarios into consideration. The demonstrator will include vehicles with advanced sensor configurations and VRU detection algorithms with the main focus on VRU detection in heavy rain and fog conditions.

The purpose of this document is mainly to support the technical coordination and monitoring of the Demo 2 development. It is therefore working as a technical document, supporting the work of the system developers throughout the process, as well as the related work that will be performed in T3.6 focusing on technical verification. This final version of the deliverable sums up the used vehicles and hardware as well as the scenario selection process which was described in detail in the previous version of this report. This report focuses on a description of three additional measurement campaigns with different purposes as well as the analysis and evaluation of their results. Here, the influence of different bad weather conditions on several sensor types are investigated and quantified in two separate activities. The first analysis, conducted by CARIAD and AUDI quantifies the effect of the tested adverse weather scenarios on both radar and video. The second one, conducted by Bosch, investigates the influence of rainy or foggy environment on the performance of LiDAR systems as well as possible instrumentation for the quantification/classification of environmental conditions. For the purpose of validating functionalities under adverse weather conditions in simulation, the weather filter which was introduced by THI in the previous report is described in its final version here.

Additional measurements to further quantify adverse weather effects as well as perception improvement measures will be conducted in the final phase of the project and reported in the upcoming Deliverable report D3.8: Verification report for Demos 2, 3 and 4.



2. Demonstrator hardware

For Demo 2, four different measurement campaigns for different investigation and evaluation purposes have been conducted. Campaign one has been reported in Deliverable report D3.2 (SAFE-UP, Deliverable report D3.2, 2021). Campaigns two, three and four are the scope of this report.

The vehicle used in the second and third measurement campaign, depicted in Figure 1, is the same vehicle that is used as Demo 3 integration platform and contains closer to series radar and video sensors with object data output (in the following referred to as *Demo 3 vehicle*). Additionally, raw data access is available for the radar sensors.

A detailed description of the Demo 3 hardware architecture and technical specifications can be found in the Deliverable report D3.1 (SAFE-UP, Deliverable report D3.1, 2021).



Figure 1: *Demo 3 vehicle*: a Bosch development vehicle with close to series radar and video sensors.

For the fourth measurement campaign, three vehicles provided by Bosch and CARIAD were used. CARIAD provided a recording and development vehicle equipped with a complete camera belt consisting of 12 cameras and required computational and storage capacities (see Figure 2). These cameras capture the full surroundings on short ranges and the vehicles forward and backward directions over long-range distances.





Figure 2: CARIAD development vehicle featuring a 360 degrees camera belt.

In order to detect and quantify environmental influences, Bosch provided a vehicle equipped with a Campbell CS125 and a Vaisala MD30 (see Figure 3). The Campbell CS125 sensor monitors present weather effects and quantifies the visibility range. It is typically used in aviation (Campbell Scientific, 2022). The Vaisala MD30 sensor records data regarding the road surface like surface temperature or water layer thickness (Vaisala, 2022). It is only recently that such sensors have been mounted onto a car, see for the fog sensor (Waymo, 2022) and the road condition sensor (Universität Ulm, 2022) (Universität Ulm, 2022) or (Bijelic, 2020), respectively.

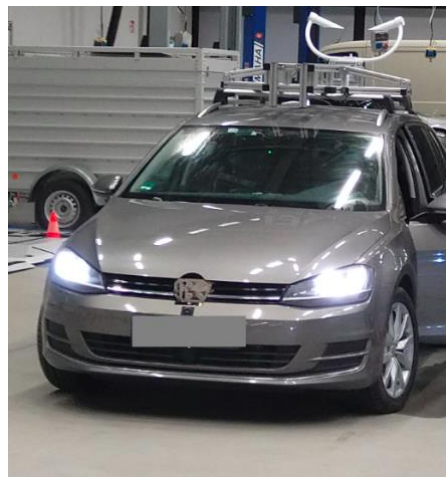


Figure 3: Bosch development vehicle equipped with road condition and visibility (mounted on the roof top) sensors.

The second Bosch vehicle, depicted in Figure 4, contains video and long range LiDAR sensors with wiper cleaning system and raw data access but without object data output.

In addition a short range LiDAR was mounted on a stationary tripod and corresponding measurements were taken in different weather conditions.



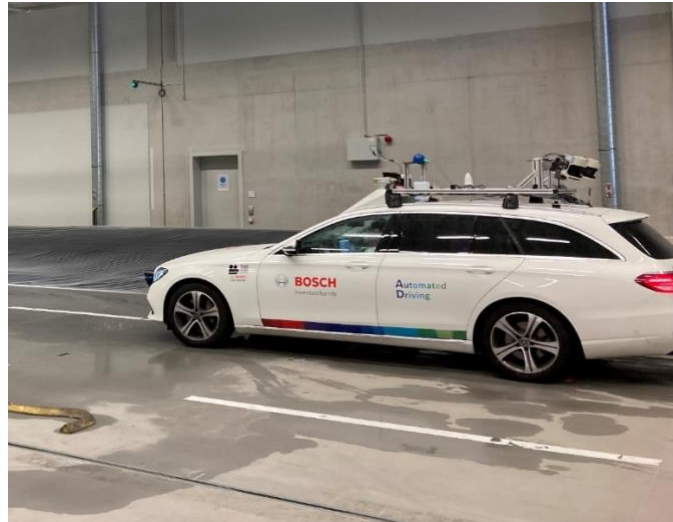


Figure 4: Bosch development vehicle with video and LiDAR sensors

3. Measurement campaigns

Following up the first measurement campaign documented in Deliverable report D3.2 (SAFE-UP, Deliverable report D3.2, 2021), three additional measurement campaigns were conducted.

The second measurement campaign (see section 3.1) is performed to assess the detection performance of state of the art/series sensor sets with a special focus on the degradation of their field of view in adverse weather conditions using static scenarios only.

The third measurement campaign (see section 3.2) uses scenarios identified from real world accident data to assess sensor performance within dynamic scenarios and is not in the scope of this deliverable but will be presented in D3.8.

The fourth measurement campaign (see section 3.3) is conducted to assess the influence of adverse weather conditions on short and long range LiDAR systems and perform initial measurements of a mechanical system to mitigate detrimental effects of adverse weather on the LiDAR performance. Additionally measurements to assess the performance of vehicle mounted instrumentation to quantify and classify weather conditions are performed.

All measurement campaigns took place in the Center of Automotive Research on Integrated Safety Systems and Measurement Area (CARISSMA). With an indoor test area of 1800 m² (100m x 18m), the CARISSMA research and test center is an essential part of automotive research at Technische Hochschule Ingolstadt.



3.1 Second measurement campaign

For the second measurement campaign, Demo 3 vehicle is used (SAFE-UP, Deliverable report D3.1, 2021), which is equipped with a radar and a camera sensor. The sensors yield data on a location of reflection (radar) and object level (camera). The processing software of the raw sensor data (received radar signals, raw camera images) runs embedded on the sensors themselves. Thus, the results depend on the performance of the applied algorithms. The goal of the measurements is to estimate the fields of view (FoV) of the radar and the video sensors, so that the results can be integrated into simulations to estimate the influence of different weather conditions and give an indication of how far today's sensors already cover their effective field under adverse weather conditions. A second aspect is the improvement of today's sensor models, which mostly only cover range and aperture angle and do not take into account general real existing effects in the sensors (e.g. optical aberrations of the camera objective or distortions of the radar signals due to interference effects from vehicle components in the proximity of the sensor).

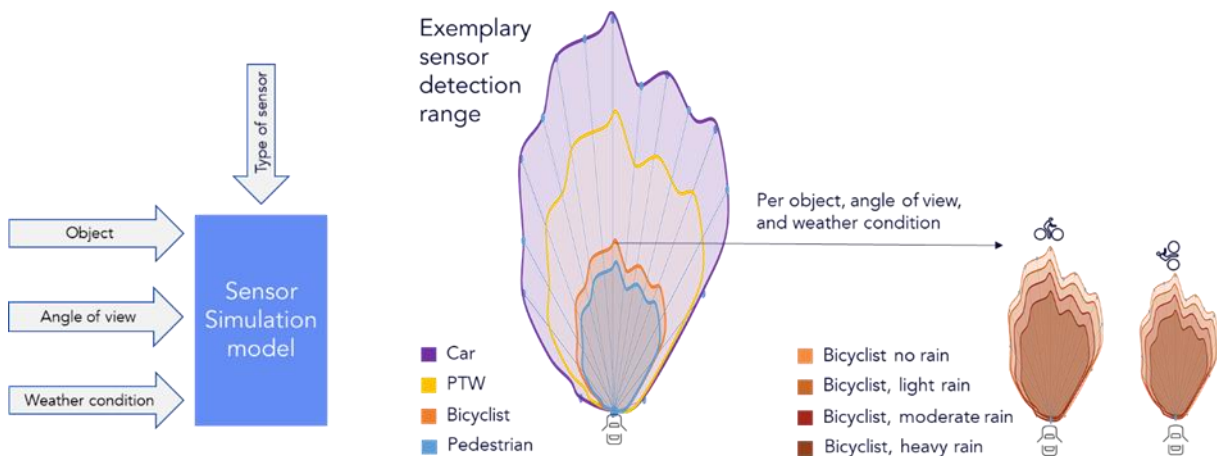


Figure 5: General idea behind the second measurement campaign for integrating sensor models in simulations.

Figure 5 shows the general idea behind the second measurement campaign. How the sensor should be modelled in simulations depends, besides other factors, on the type of sensor, the object, the angle under which the object is seen by the vehicle, and the weather condition. Therefore, the tests focus on these influencing factors on the FoVs. An example of how the resulting FoVs for different objects can look like, is shown in Figure 5 for a vehicle, a PTW, a bicyclist, and a pedestrian, whereby for the bicyclists more detailed differences based on the rain intensity and the angle of view are shown in addition. To reduce the testing effort in this measurement campaign, the focus was on an angle setting, which is representative for crossing objects, and on the three VRU types. For these conditions, a grid of locations was set up, where dummy targets from 4active systems GmbH (4A) (see Figure 6) were placed in different distances and angles to the vehicle.





Figure 6: Investigated dummies from 4A in the second measurement campaign

As the rain area in the test hall is limited to 50m x 4m, the setup is rotated such that the vehicle's investigated sensors as well as the waterproof dummies are within the rain area. Also, the targets are rotated at these locations such that the angle between the vehicle and the target direction always maintains 90 degrees, which is realistic for crossing scenarios. Figure 7 shows the grid of static measurement locations as well as how the rotation is realized on the example of the 33° positions.

Following configurations in all combinations are tested in the second measurement campaign:

- Targets: Pedestrian (moving legs), bicyclist (static), powered two-wheeler (static)
- Weather settings: Dry, rain 16mm/h, rain 66mm/h, rain 98mm/h, fog 25 - 35m visual range, fog with <10m visual range
- Angle between vehicle's forward direction and target position: 0°, 16°, 33°, 50°
- Radial distances from vehicle's front to target position: 7.33m, 14.7m, 22.0m, 29.3m, 36.7m, 44.0m



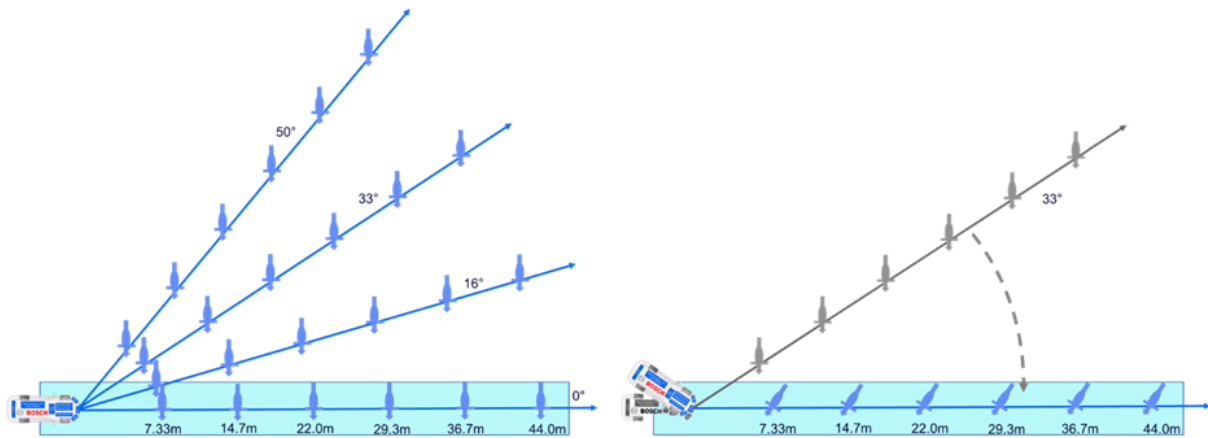


Figure 7: Test grid of the second measurement campaign (static measurements) inside the CARISSMA test hall

3.2 Third measurement campaign

The focus of the third measurement campaign is on dynamic tests under rainy weather conditions to generate data to verify the simulative results with real world performances in adverse weather conditions. To be able to verify simulated results with real world performances in adverse weather conditions, scenarios must be identified that are testable in a test hall under replicable conditions. The method for selecting the scenarios for the test hall is described in detail in the Deliverable report D3.2 (SAFE-UP, Deliverable report D3.2, 2021). In a first step, the required space for testing the four use cases for car-to-VRU crashes under adverse weather conditions identified in (SAFE-UP, Deliverable report D2.6, 2021) was compared to the test hall boundary conditions. For the scenario clusters assessed as testable in the test hall, the speeds of the VRUs and vehicles are further analysed. As an outcome of the analysis, one speed configuration was defined based on crashes involving killed or seriously injured (KSI) road users and another speed configuration based on all crashes involving injured road users. Depending on the defined speeds and the test area, possible Time-to-Collision (TTC) periods are calculated to define how long the scenario can be approximately tested while remaining in the rain area. The resulting scenarios selected for testing in the THI test hall, are summarized in Table 1.



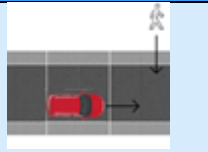
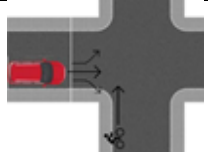
| C2P/C2B conflict scenario | Schematic illustration of conflict situation | Vehicle speed | Target speed | Possible TTC |
|---------------------------|---|----------------------|--------------------------------------|--------------|
| P-CLwoSO |  | 48kph (KSI) | 8kph (Running adult) (ASPECSS, 2014) | 2sec |
| | | 43kph (All injuries) | 5kph (Walking adult) (ASPECSS, 2014) | 2-3sec |
| B-CR |  | 26kph (KSI) | 15kph (KSI) | 1sec |
| | | 15kph (All injuries) | 15kph (All injuries) | 1sec |

Table 1: Summary of selected scenarios for Demo 2 with suggestions for test speeds and TTCs.

Testing of the defined scenarios in the test hall was performed using the Demo 3 vehicle, a 4A pedestrian target, a 4A bicyclist target, and a 4A target moving system (including a belt, propulsion system, and a reverse plate).

Due to limitations of the test hall (possible driving area of the test vehicle, rain area, run-off/safety space within the hall, possible placement of technical equipment) the P-CLwoSO scenario had to be mirrored (changed to crossing pedestrian from right). This does not hamper the validity of the measurement results as all sensors are mounted along the vehicles longitudinal axis and feature no particular asymmetries in the azimuthal detection characteristics.

To ensure that the vehicle is not able to detect the target before the specified TTCs and especially not before the sensors have fully entered the rain area, a sight obstruction wall is installed and positioned scenario-specifically as depicted in Figure 8 and Figure 9.



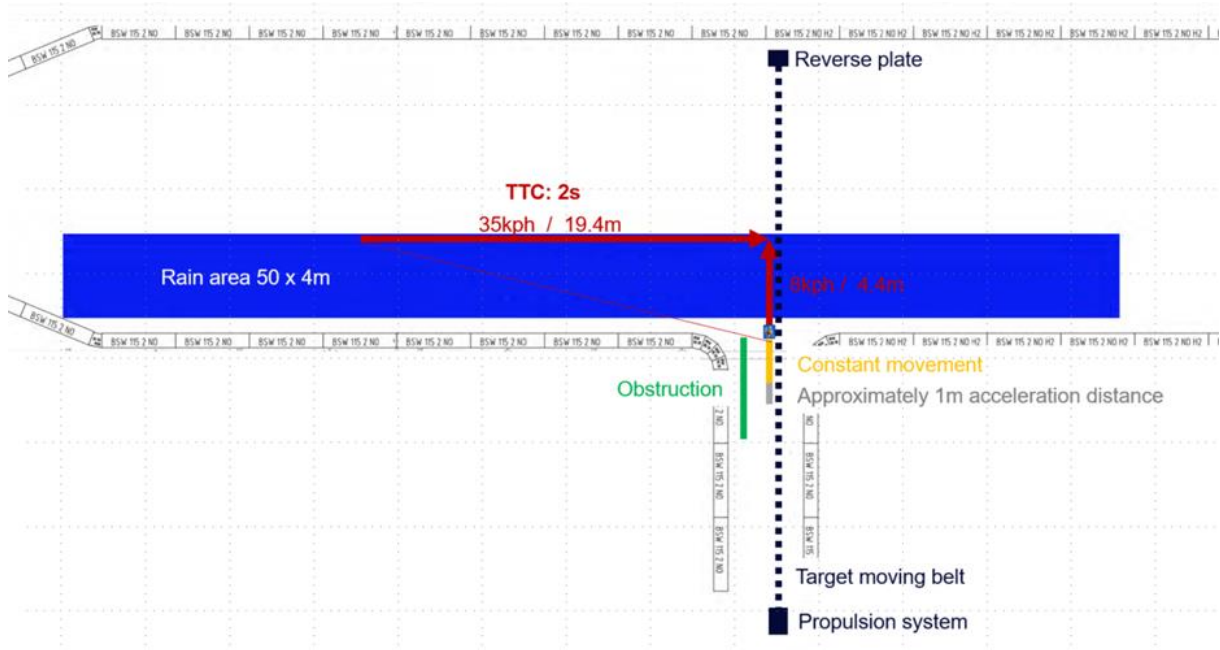


Figure 8: Measurement setup on the example of a mirrored scenario from cluster P-CLwoSO (35kph vehicle velocity, 8kph pedestrian velocity, and a TTC of 2s)

For safety reasons (to ensure the controllability of the vehicle for the test driver also under rainy conditions in the test hall), the tests were performed starting from vehicle speeds significantly below the speeds specified for the test scenarios and increased incrementally as close to the scenario speeds as possible. Reaching the specified test speeds was not possible due to the test hall limitation for all scenarios. Table 1 lists the set of actually performed scenario measurements.

| Target | Scenario | Rain setting | Impact point | Vehicle velocity | Target velocity |
|------------|----------|----------------------------|--------------|-----------------------|-----------------|
| Pedestrian | P-CLwoSO | [0,16mm/h, 66mm/h, 99mm/h] | 50% | [15kph, 30kph, 35kph] | 8kph |
| Bicyclist | B-CR | [0mm/h, 16mm/h] | 50% | 25kph | 15kph |

Table 2: Tested configurations in the third measurement campaign

In Figure 8 the resulting configuration for the pedestrian on the example of 35kph vehicle velocity, 8kph pedestrian target velocity, and a TTC of 2s is shown.



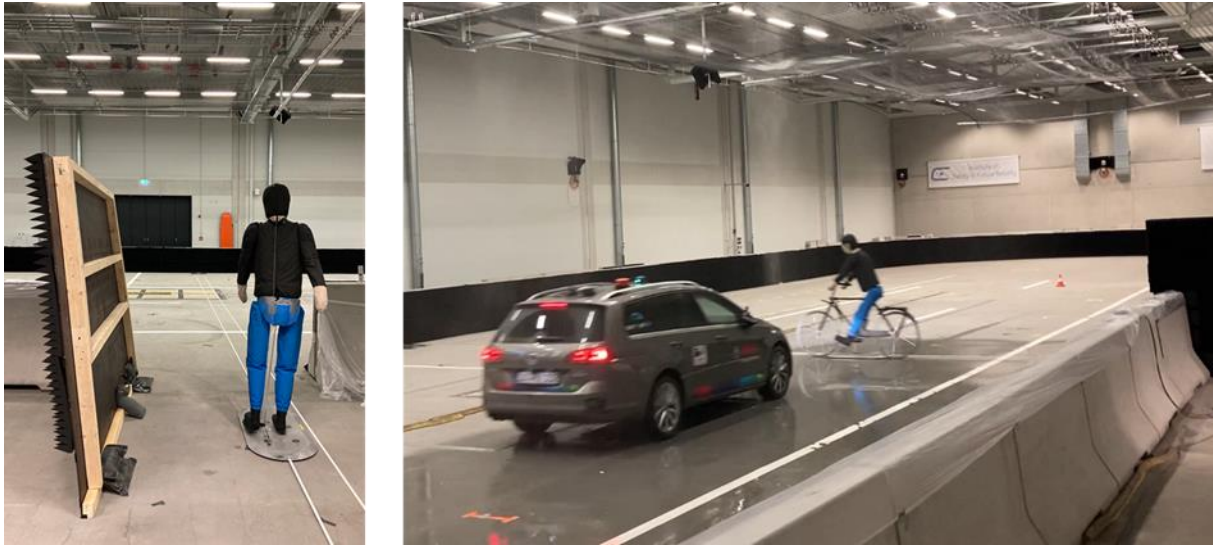


Figure 9: Images of the third measurement campaign

The results of the measurements evaluation and the comparison to the simulation are part of Task 3.6 in SAFE-UP and will be presented later in Deliverable 3.8.

3.3 Fourth measurement campaign

The fourth measurement campaign has two objectives.

The first objective is to understand the performance of LiDAR sensors for point cloud data under different weather conditions for environmental perception of autonomous and highly automated driving vehicles. Two different LiDAR sensors were taken for the analysis.

1. Short Range LiDAR – Hesai
2. Long Range LiDAR – Bosch

Test case Scenario

The test cases were performed under stationary conditions with stationary target and stationary sensor across three environmental conditions.

- Dry
- Fog
 - Short Range LiDAR (at 10 m visibility range)
 - Long Range LiDAR (10 m – 140 m visibility range)
- Rain
 - Short Range LiDAR (at 32 mm/h)
 - Long Range LiDAR (32 mm/h, 82 mm/h)







| | | |
|--------------------------|---|--|
| Scenario | Stationary evaluation | |
| Sensor | Mounted on fixed frame (Hesai) | |
| Object | Lambertian target (reflectance 10 %) and retroreflective target - RA3 (Yellow), RA2(Stop) | |
| Environmental conditions | No rain | Rain rate 32 mm/h |
| |  |  |
| | Fog from 10 m – 1500 m visibility | |
| | 10 m visibility | 1500 m visibility |
| |  |  |

Table 3: Target under different weather conditions

Scenario 1: Dry

In this scenario, measurements are performed with a short range LiDAR on stationary targets in dry environment. This forms the basis or reference for comparison against other weather conditions.

Scenario 2: Fog

In this scenario, measurements are performed with a short range LiDAR on stationary targets in fog. For this measurement, the fog is increasingly condensed so that the visibility clears up from 10 m visibility to more than 1500 m visibility. Figure 10 shows the setup of target and sensor for a pictographic scene understanding.

Scenario 3: Rain

In this scenario, measurements are performed with a short range LiDAR on stationary targets in rain at rain intensity of 32 mm/h. The pictographic scene is showed in Figure 10.



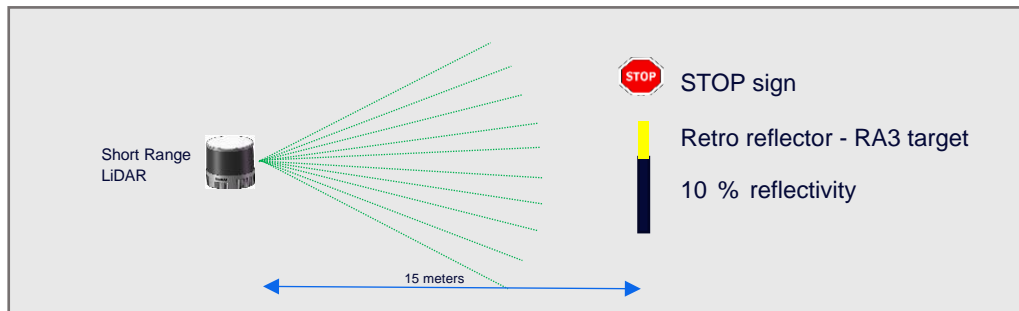


Figure 10: Graphical representation of Short Range LiDAR scenario setup

Scenario 4: Fog

In this scenario, measurements are performed from a long range LiDAR on stationary targets with different optical properties in fog. For this measurement, the fog is increasingly condensed so that the visibility clears up from 10 m to more than 1500 m. The Figure 11 shows the setup of target and sensor for a pictographic scene understanding.



| | | |
|--------------------------|--|--|
| Scenario | Stationary evaluation | |
| Sensor | Mounted on stationary car | |
| Object | Stationary retroreflective target (RA3) and Lambertian target (reflectance 10 %) | |
| Environmental conditions | Fog from 10 m – 1500 m visibility | |
| | <p>10 m visibility</p>  | <p>1500 m visibility</p>  |

Table 4: Target in Fog



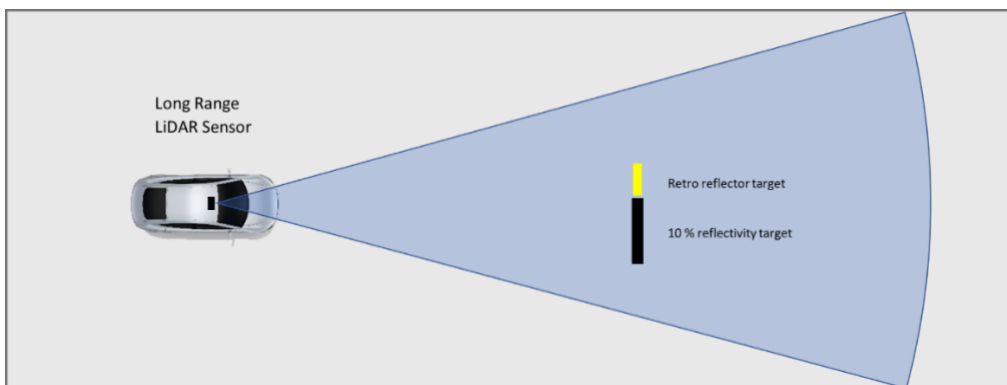


Figure 11: Graphical representation of Long Range LiDAR scenario setup

Scenario 5: Rain

In this scenario, measurements are performed from a long range LiDAR on stationary targets with different optical properties in rain. At the beginning, a reference measurement is performed without rain. Afterwards, a measurement is performed in rain at a rain rate of 32 mm/h, which is then repeated at an increased rain rate of 82 mm/h. The pictographic scene is showed in Figure 11.

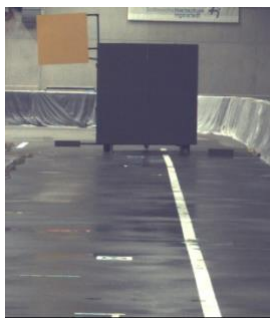
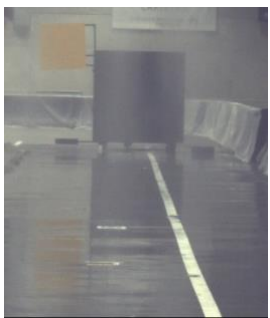

| | | | |
|--------------------------|--|---|--|
| Scenario | Stationary evaluation | | |
| Sensor | Mounted on stationary car | | |
| Object | Stationary retroreflective target (RA3) and Lambertian target (reflectance 10 %) | | |
| Environmental conditions | No rain  | Rain rate 32 mm/h  | Rain rate 82 mm/h  |

Table 5: Target in Rain

The second objective of this measurement campaign is the validation of both a fog and a road condition sensor to be used as ground truth sensors while driving.

For this objective, development vehicles from CARIAD and Bosch (see section 2 and Figure 2 and Figure 3, respectively) were utilized: In the first measurement drive the vehicle with mounted fog sensor is driving repeatedly through the 50 m long and 6 m wide part of the hall



which is intended for fog experiments. The aim is the comparison of the measured visibility range of a stationary fog detector and the fog sensor, mounted on a driving car.

For the second experiment, comprising the testing of the road condition sensor, different rain strengths and fog scenarios are configured. This allows to analyze the characteristics of road condition sensor and the interplay with the mounted fog sensor under different conditions. The secondary objective is the recording of data in adverse weather conditions with the entire camera belt of the recording vehicle. To this end also stationary targets and luminous targets are placed along the test track. Moreover, the recordings have been performed under different lighting conditions, which however, are not calibrated. Note that this data is not suitable for the training of CNNs since the data only shows low variance in an artificial scene.



4. Demo 2 development

4.1 Overall demonstrator scope

The overall scope of Demonstrator 2 is to both quantify and optimize VRU detection for safe object detection in real-world scenarios in all weather conditions, with the main focus on VRU detection in heavy rain and fog.

To achieve this goal, special focus is given to an understanding of the relevant weather effects on different sensor types, as well as the modelling of these effects for simulations as a first step. The results of this analyses and the developed simulation models will be detailed in the following sections.

4.2 Results of the second measurement campaign

This section details the evaluation of the second measurement campaign and the method for generating FoVs for the investigated front radar sensor and the front video sensor from Bosch, which can be integrated in simulations. In order to be able to interpret and relate the results, the outcomes of the measurement campaign are compared with the theoretical characteristics of the sensors. In addition, because of the spatial limitations of the test hall rain area to about 45m, a statement about the detectability outside the measurement field can be made with the help of the theoretical limits. The focus of the shown results is on pedestrians and on precipitation as it is significantly more prevalent in crashes with VRUs than other weather phenomena like fog.

4.2.1 Evaluation Front Radar Sensor

4.2.1.1 Filtering of Radar Locations

The radar sensor calculates the positions of radar reflections (called radar locations in the following) in a spherical coordinate system and yields those positions together with estimates of the reflection properties of the reflecting object and an estimate of the quality of the position calculation.

Before the radar locations are used for a threshold-based detection decision, they are filtered by their quality estimates. Therefore, in a first step all radar locations are discarded, whenever their estimated azimuthal position quality is below 0.75 (*Quality* is a sensor specific measure to quantify the estimated uncertainty of the estimated position on a scale from 0.0 (highest uncertainty) to 1.0 (lowest uncertainty)). In a second step, all radar locations are discarded, when their estimated radar cross section (RCS) is below or equal to -20dBm^2 , to ensure that only reflections possibly originating from a VRU are considered.



These filtering characteristics are provided by Bosch radar development departments and represent typical characteristics for radar VRU detection.

4.2.1.2 Correction of Target Positions

Ideally, the positions of the vehicle and the targets in the measurements would have been exactly as described in section 3.1. Nevertheless, when analysing the results of the measurement, it was obvious that for some configurations the relative positioning of vehicle and detection target significantly differed from the original plan. The positioning of the targets was performed using markers on the ground. Here it can be assumed that no placement errors were made that would have had a significant influence. The positioning of the vehicle was performed by manually “parking” the vehicle, which was guided by a laser. Positioning of the vehicles longitudinal axis with an error of only 1° leads already to an offset of 0.75m at the last target position at 43m. Due to that errors, in the vehicle rotation need to be identified in data post-processing, before a threshold-based detection decision is executed.

Hence, the radar locations are filtered such that the error in radial direction is smaller or equal to 1m, because the error in distance between the vehicle and the target is assumed to be small. Then, histograms of the radar location counts at different angles are created, where the nearest and second nearest local maxima to the expected angle are extracted. If for at minimum 4 of out the 6 tested target positions at one angle, the local maxima have a systematic offset from the expected angle, the angles are adjusted. In Figure 12, the histogram of the angles of the radar locations from position 1 (7.33m distance) and 3 (22.0m distance) are exemplarily shown for the configuration of a pedestrian target placed at a desired angle of 16° . At both positions, the nearest local maximum is at 18° instead of the originally planned 16° . As this offset was in total seen at 5 out of 6 positions, the angle was adjusted to 18° with which the reference position of the target is calculated in a later step. Table 6 summarizes which angles need to be corrected for the pedestrian and rain tests. As the adjustment of the rain system is time consuming, the tests with all the targets, angles, and positions were conducted at one rain intensity before the tests for the next rain intensities started. For this reason, there are no correlations of angular deviations between different precipitation intensities and same angles, but correlations could be found between the different tested targets.



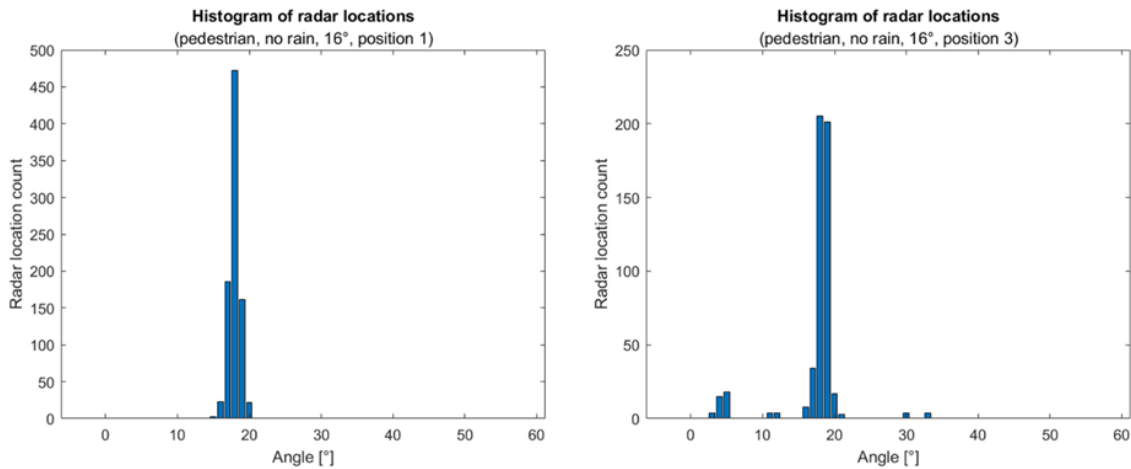


Figure 12: Example histograms of the angles of the radar locations for position 1 and 3 (pedestrian, no rain, desired angle: 16°). At both positions, the nearest local maximum is at an angle of 18° instead of the originally planned 16°.

| <i>Target</i> | <i>Weather</i> | <i>Desired Angle</i> | <i>Corrected Angle</i> |
|-------------------|----------------|----------------------|------------------------|
| <i>Pedestrian</i> | 0mm/h | 0° | 1° |
| <i>Pedestrian</i> | 99mm/h | 0° | 1° |
| <i>Pedestrian</i> | 0mm/h | 16° | 18° |
| <i>Pedestrian</i> | 16mm/h | 16° | 17° |
| <i>Pedestrian</i> | 0mm/h | 33° | 30° |

Table 6: Summary of the angles, which were corrected for the pedestrian tests in dry and rainy settings.

4.2.1.3 Theoretical Field of View

This section details the theoretical characteristics of the radar sensor, which is later aligned with the measurement results. The FoV of the investigated radar sensor is displayed for an RCS value of 10m² and nominal conditions in Figure 13 on the left hand side. The theoretical FoV is particularly used to make assumptions about the detectability outside the measurement field and in between the measurement locations. As the theoretical FoV is fit in the next steps to the measurement locations, especially the shape rather than the scaling is important. As a preparatory step, the given FoV is transformed from polar coordinates to vehicle-fixed Cartesian coordinates as shown in Figure 13 on the right hand side. In this coordinate system, the origin is at the front radar location, the x-axis is aligned in longitudinal direction, and the y-axis in lateral direction from the vehicle perspective.



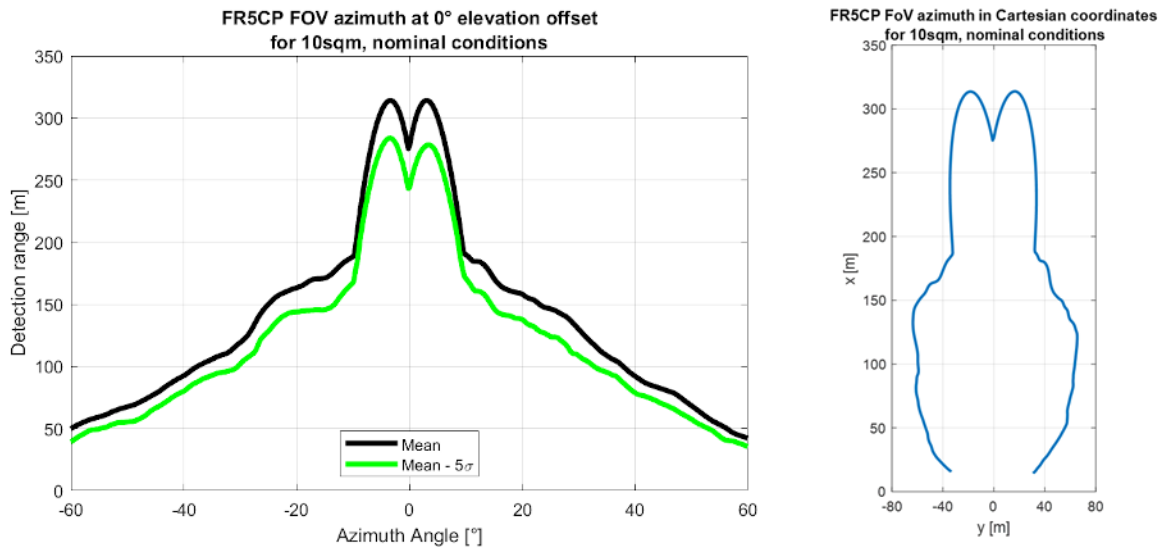


Figure 13: FoV in polar and Cartesian coordinates for 10sqm and nominal conditions (Robert Bosch GmbH, 2022)

4.2.1.4 Detection evaluation of the measurement campaign (radar, pedestrian, rain)

To decide in a threshold-based approach if a target is detected or not, a bounding box around the reference position is calculated. Radar locations within the volume enclosed by this bounding box are evaluated as detections. The reference positions of the target are calculated using the corrected angles identified in section 4.2.1.2. Figure 14 shows for two examples the reference position of the target with the used bounding box when the angle is not corrected (first row) and when the angle is corrected (second row). It is obvious from the images that the correction is necessary and the deviation of the radar locations from the reference position increases with higher distances to the vehicle.

The bounding box for the pedestrian is chosen as a cylinder shape with a height of 2m and a radius of 0.5m. Therefore, radar locations are counted as referring to the target, only if they have a distance in the x- and y-plane less than or equal to 0.5m to the (corrected) reference position of the target and a z-coordinate value between or equal to -0.7m and 1.3m. The origin of the z-axis is at the radar mounting elevation, located at approximately 0.65m above the ground. If at least one radar location meets all criteria, the pedestrian is classified as detected. In Figure 15, the radar locations for the pedestrian target at a rain intensity of 16mm/h are shown for position 3 and 4 at 33°. As radar locations are within the bounding box for position 3, the pedestrian is classified as detected at this position. For position 4 no radar location is within the bounding box, which is why the pedestrian is classified as not detected at this position.



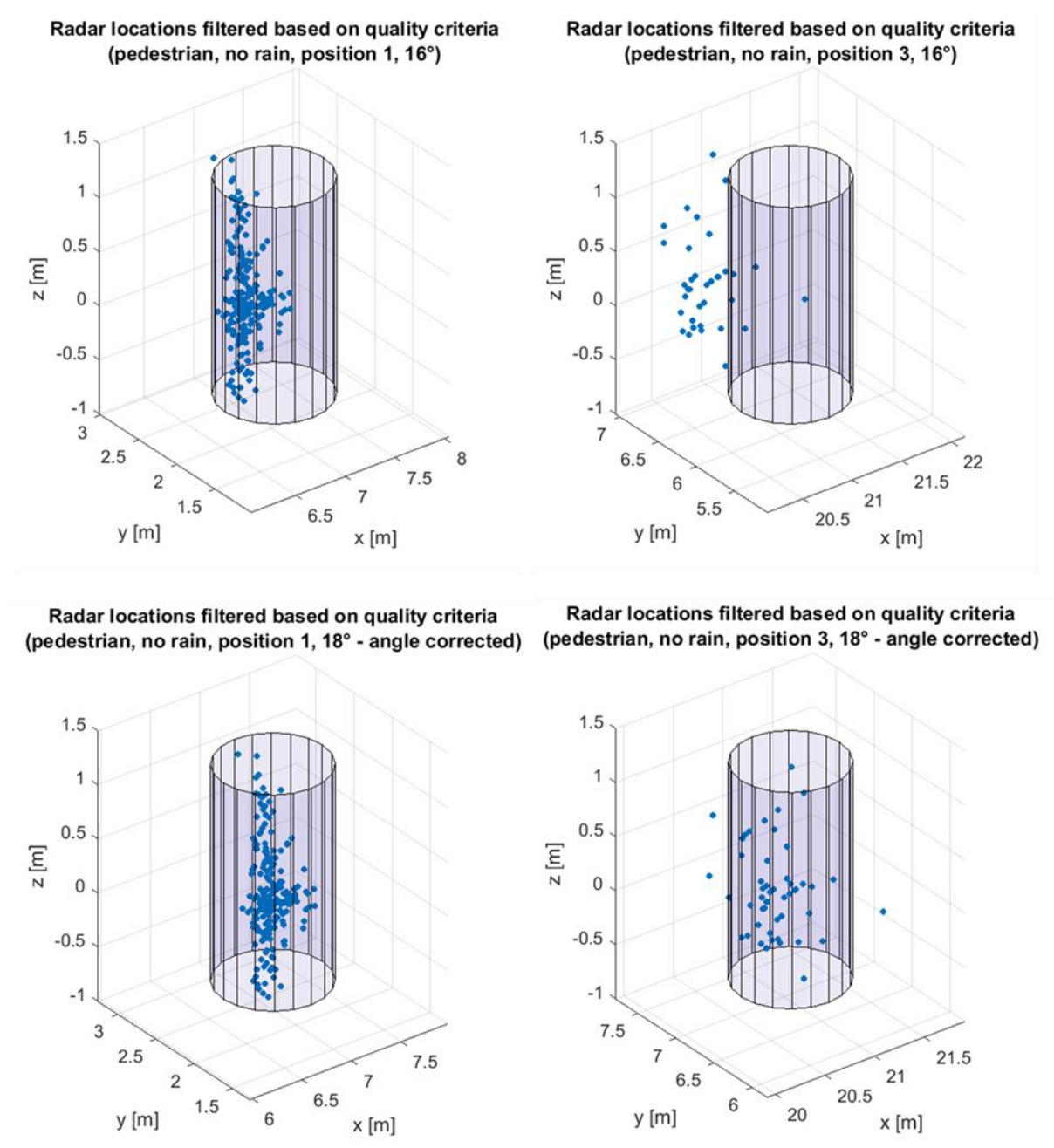
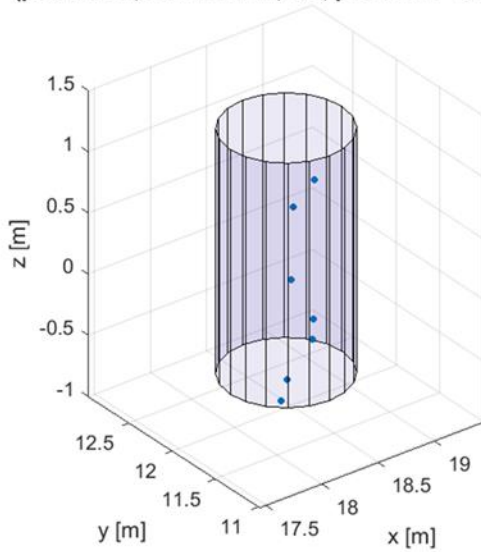


Figure 14: Location of the used bounding box for the pedestrian target at two positions when the angle is not corrected (first row) and when the angle is corrected (second row).



This project has received funding from the European Union's Horizon 2020 research and innovation programme under Grant Agreement 861570.

Radar locations filtered based on quality criteria (pedestrian, rain 16mm/h, 33°, position 3 - detected)



Radar locations filtered based on quality criteria (pedestrian, rain 16mm/h, 33°, position 4 - not detected)

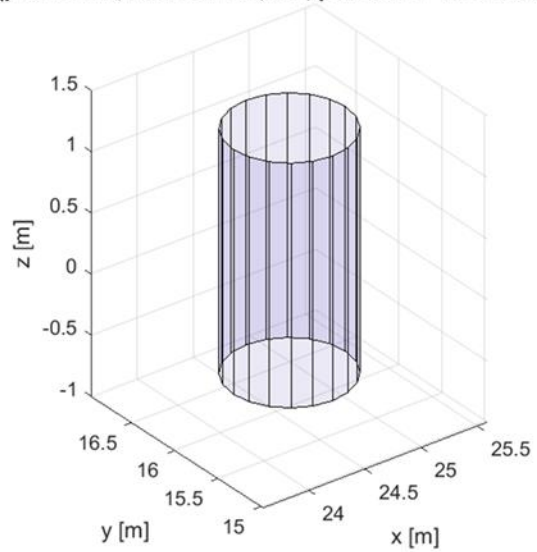


Figure 15: Detection decision for two example positions of the pedestrian target at a rain intensity of 16mm/h.



The full grid at which positions the pedestrian is classified as detected is exemplarily shown in Figure 16 for dry conditions and the results for the different rain settings are displayed later in Figure 17.

The pedestrians classified as detected are marked with measuring points in green. The non detected pedestrians are displayed with red dots. With this data, the detection range of the sensor can be estimated in the measured area, but for greater distances no measured values are available as the furthest measuring point was accordingly at 43m.

The measurements regarding the detectability under different ranges and detection angles are conducted in the rain area, which has an extension of 50m x 4m and can be configured with different rain intensities. However, this area could not be used completely in front of the vehicle, as the vehicle must be in the rain area at least up to the camera sensor mounted behind the windshield. Due to these limitations, no data beyond 45m was recorded, although it can be assumed that the pedestrian would have been detected here at least without rain. Therefore, the following chapter shows an approach for combining theoretical FoVs with the measured data to generate also assumptions for non-tested areas.

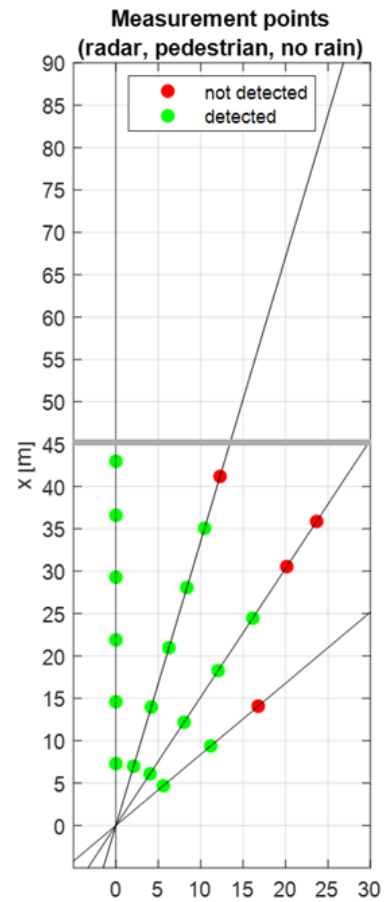


Figure 16: Grid of detected and not detected positions for the pedestrian target for dry conditions.

4.2.1.5 Fitting of the Theoretical Field of View to the Measurement Results

To generate FoV, which are not limited to the testable area from the test hall, theoretical characteristics of the radar sensor are combined with the results from the measurement campaign. Therefore, the theoretical shape of the FoV is used and scaled such that it matches the measured values categorized in detected or not detected as closely as possible. Even if it is not always possible to separate them strictly, the aim was to fit the shape such that the green marked dots are inside the FoV of the radar, and the red points outside. The theoretical FoV if fitted to the data under the assumption that rain has the same influence in every direction. This is done by scaling the FoV radially from the origin (relation of x- and y-coordinates is kept constant) such that as many non detected positions as possible are outside the scaled FoV and as many detected positions as possible are within the scaled FoV. Besides minor deviations due to uncertainties in edge areas, the FoVs shown in Figure



17 are determined for the different rain intensities, which can be further used, for example, in simulations to model the influence of rain on the radar.

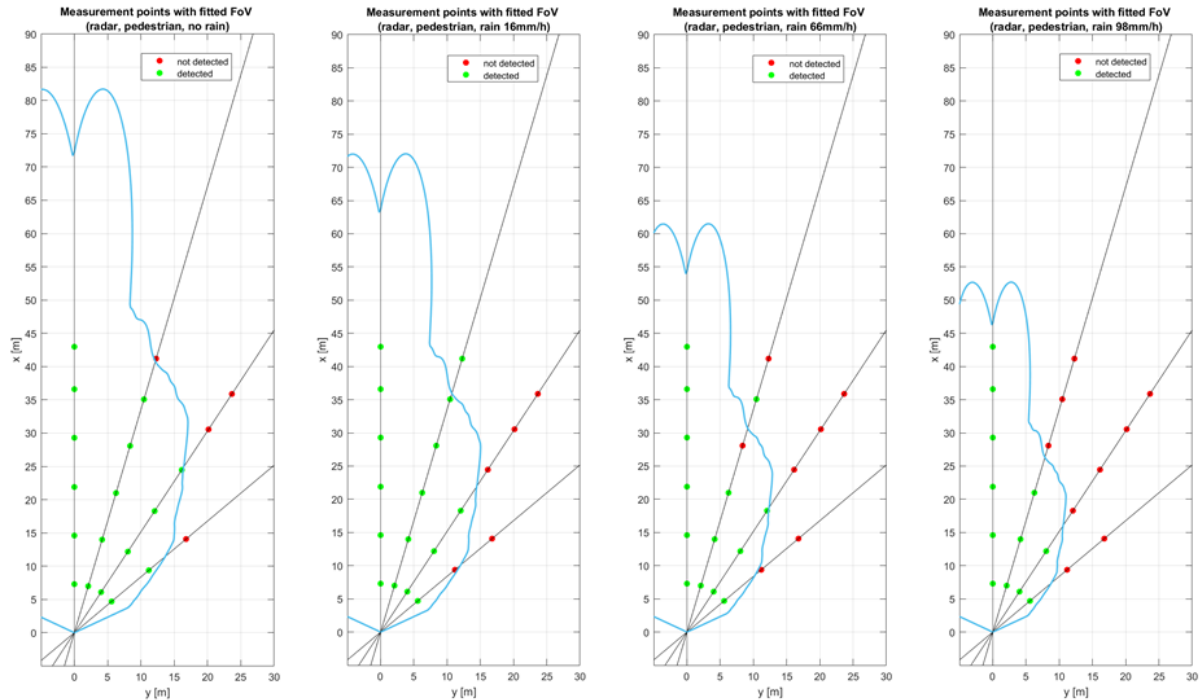


Figure 17: Measurement points with fitted FoVs for the radar sensor, the pedestrian target and different weather settings

4.2.2 Evaluation Front Video Sensor

This section describes how the data from the second measurement campaign of the video sensor is evaluated in alignment with the method for the front radar.

4.2.2.1 Theoretical Field of View

The technical data of the front video sensor mounted behind the windshield in the Demo 3 vehicle is described in (SAFE-UP, Deliverable report D3.1, 2021). The image sensor used for the mono camera has 3328 pixels.

The camera evaluates the raw information of the sensor pixels differently for two different detection areas. The two modes shown in Figure 18 on the left side are called Far view mode (A) and Wide view mode (B). Each of these modes uses different resolutions of the sensor to limit the computing power consumption of the processing unit. The visualization in Figure 18 on the right shows the image of the two modes of the sensor.



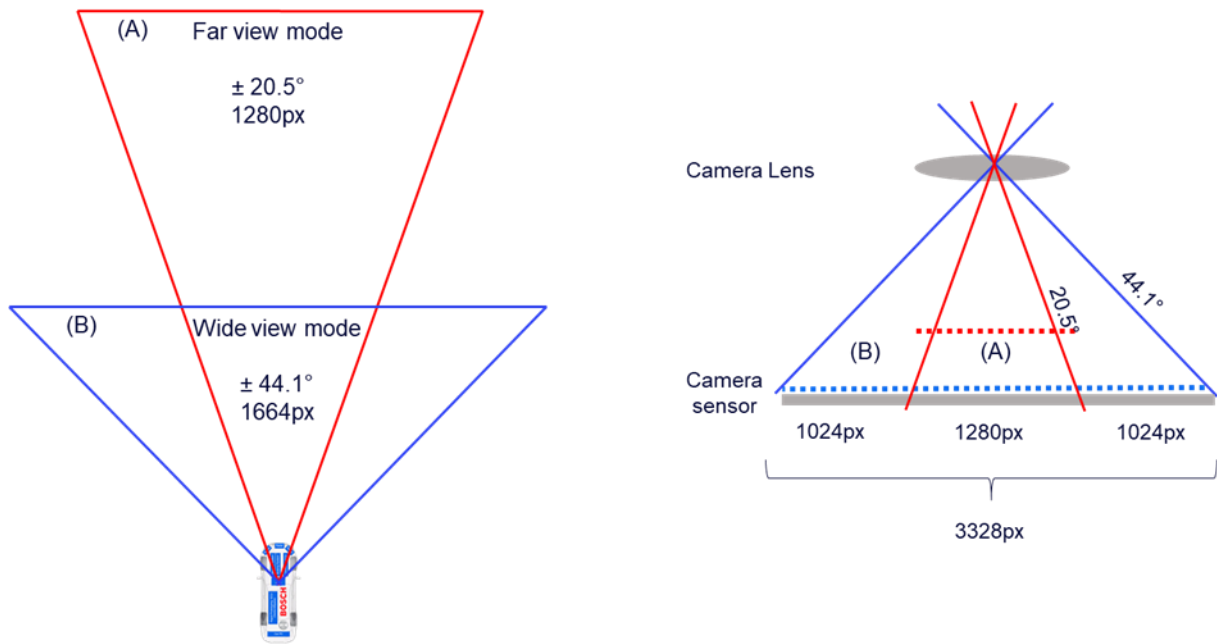


Figure 18: Visualization of the two different camera modes

In the following, the characteristics of the two different modes are described:

Far view mode:

In this area, all pixels of the sensors far view mode are used and further processed in a section of approximately 41°. Therefore, 1280 pixels are used in a high resolution of $41^\circ / 1280 \text{ px} = 0.033^\circ / \text{pixel}$ in the far view mode, which enables a significantly higher range in this area.

Wide view mode:

In this mode, however, only half of the pixels are used to save memory resources and computing power. Hence, half of the sensor pixels of 3328 corresponds to 1664 pixels, which leads to a resolution of $88.2^\circ / 1664 \text{ px} = 0.053^\circ / \text{pixel}$ in the wide view mode. However, this resolution is sufficient for the detection performance as the objects are larger due to the smaller distance to the lens on the sensor.

General assumptions for the detectability of objects when using a mono camera

Because of the half resolution in the wide view mode compared to the image resolution in the far view mode (A), the maximum detection range in the wide view mode is almost halved (B). The detection performance in the far view mode reaches the maximum in the middle of the image. In the boundary area of the two modes, the detection facilitation is considered to be fulfilled at about half of the maximum detection range of the respective mode (D) (see Figure 19: Visualization of assumed effects on the detectability (left) and the chosen interpolation points (right)).



In addition, there will be restrictions of detection in the corner areas (C) (see Figure 19). Towards the corner of the image, the detection performance of an optical lens decreases due to the diffraction and blurring behaviour.

However, static tests still have to take into account the limitations of a test hall, which can lead to a further reduction in detection performance.

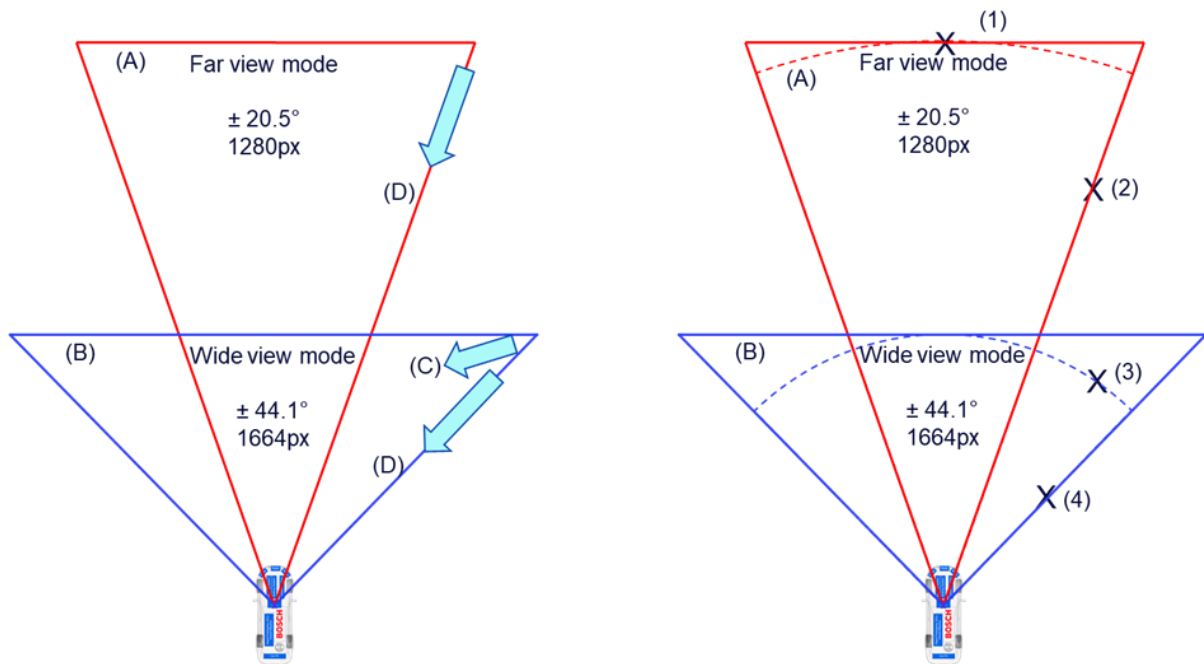


Figure 19: Visualization of assumed effects on the detectability (left) and the chosen interpolation points (right).

Determination of interpolation points

From the requirements A-D a curve will be fitted which represents a theoretical detection range with the used video sensor and its two different modes. Within the area, it is assumed to be possible to detect an object.

The points (1-4) shown in Figure 19 on the right are selected for interpolation as it is assumed that they model the different effects on the detectability (A-D).

Based on previous experience with the camera, a pedestrian detection is possible under normal, dry conditions at the full resolution of the sensors up to 70m. Therefore, the curve will be normalized to 70m, but scaled based on the measurement results in the following.

Interpolation and transformation in the vehicle coordinate system

Based on the previous assumptions, the locations of the grid points (1 - 4) are determined as follows, where the value pairs for the aperture angle and the range are given by:

angle_points = [-44.1, -32.3, -20.5, 0, 20.5, 32.3, 44.1];



`range_points = [17.5, 35, 52.5, 70, 52.5, 35, 17.5];`

Through these points in the polar coordinate system a 6th degree polynomial function is fitted. Thereby, a curve is obtained, which is shown in the left picture for the angle values from -44.1° to 44.1°.

With the resulting parameters, the assumed FoV of the sensor is obtained after the transformation into the Cartesian coordinate system. This FoV is still converted into the vehicle coordinate system and at the same time shifted in x-direction by 1.63m to the position of the camera behind the windshield. In the right picture of Figure 20, it can be observed that the resulting curve moves maximally along the ideal corner data of the camera but takes into account the practical limitation of optics and detection power.

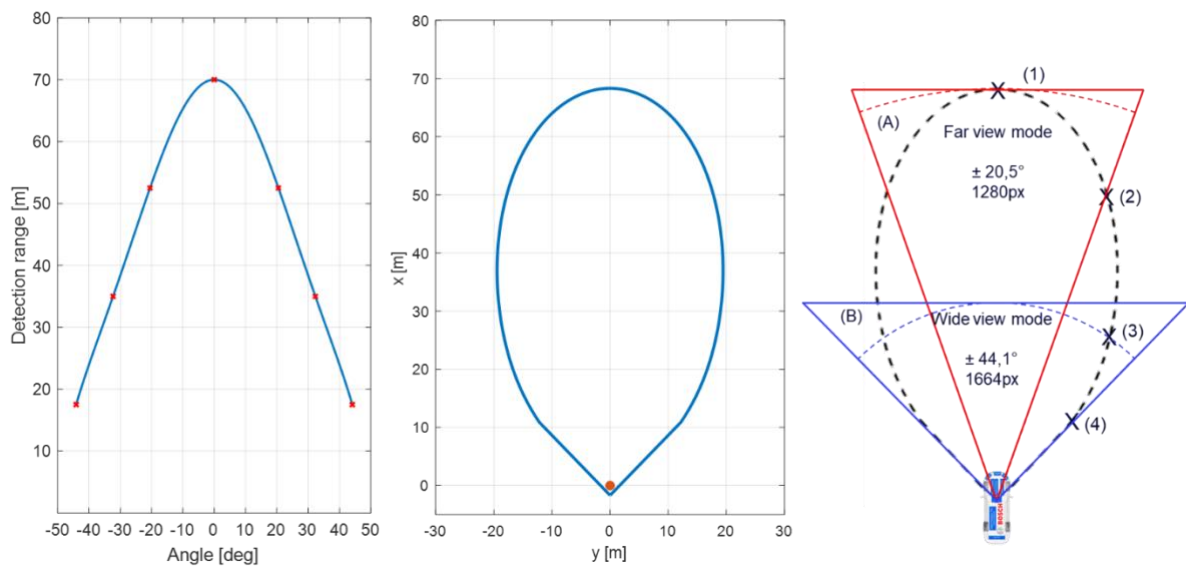


Figure 20: Fitted polynomial function in polar coordinates and transformation to the vehicle coordinate system.

4.2.2.2 Detection evaluation of the measurement campaign (camera, pedestrian, rain)

For the front video sensor, a detection algorithm which returns object lists was running in the measurement campaign. These lists can be used to decide if the pedestrian target was detected or not detected.



Firstly, the reference positions of the target are calculated, where the corrected angles identified based on radar data in section 4.2.1.2 are here also taken into account. Then the object with the nearest point to the reference position in the x- and y-plane is determined. If the error in y-coordinate direction is smaller or equal to 0.60m and the error in x-coordinate direction is smaller or equal to 3.0m, the pedestrian is classified as detected at this position. The reason why the acceptable error in the x-coordinate direction is chosen significantly larger is that the camera has difficulties in estimating the distance for stationary tests. If the vehicle would move, smaller errors can be assumed. This finding is again described in the limitation section of this chapter.

The full grid at which positions the pedestrian is classified as detected with the camera is exemplarily shown in Figure 21 for dry conditions. The results for the different rain settings are displayed later in Figure 22.

As the same restrictions on the measurement area apply for the radar and for the camera, in the following chapter, the theoretical FoVs of the camera are combined with the measured data to generate also assumptions for non-tested areas.

Measurement points with fitted FoV (camera, pedestrian, no rain)

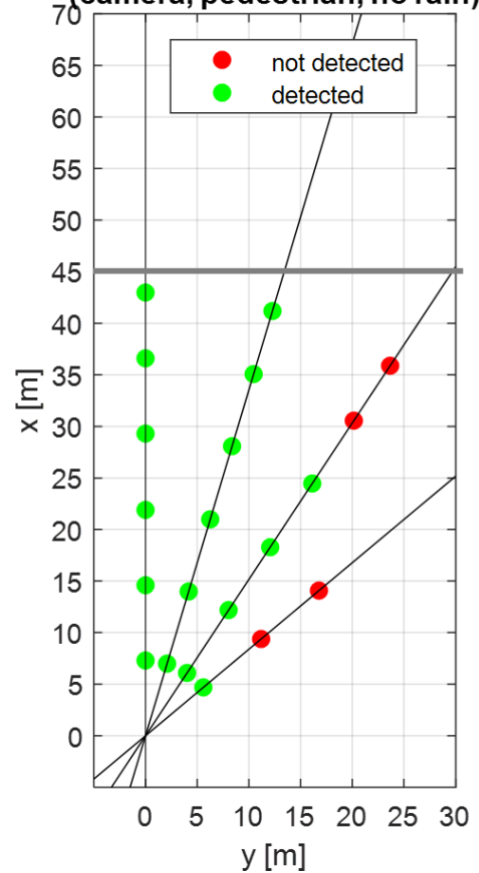


Figure 21: Grid of detected and not detected positions for the pedestrian target for dry conditions.

4.2.2.3 Fitting of the theoretical FoV to the measurement results

In correspondence to the approach for the radar, for the front video sensor the theoretical shape of the FoV from section 4.2.1.3 is used and scaled using the same method as described in section 4.2.1.5. The results thereof are shown in Figure 22 for dry conditions and the different rain intensities. While for dry conditions and the rain intensity of 16mm/h the theoretical FoV can be scaled without mismatches to the measured positions, the FoV at 66mm/h has at 0° the first two positions included, which are classified as not detected. However, it can be assumed that a pedestrian would also have been detected at these positions under dynamic conditions as test objects were successfully detected at positions in a greater distance. In the evaluation of the tests for the rain intensity of 98mm/h, too few detected measurement points are available. Because these also do not match the theoretical assumptions, no FoV can be fitted here.



When testing the camera under extremely high rainfall conditions such as 66mm/h and 98mm/h, it is noticeable that just in the middle and close to the vehicle the pedestrian target is not detected. For the development status of this camera, it could be that pedestrians directly in front of the vehicle under such rainy conditions probably have not yet been trained.

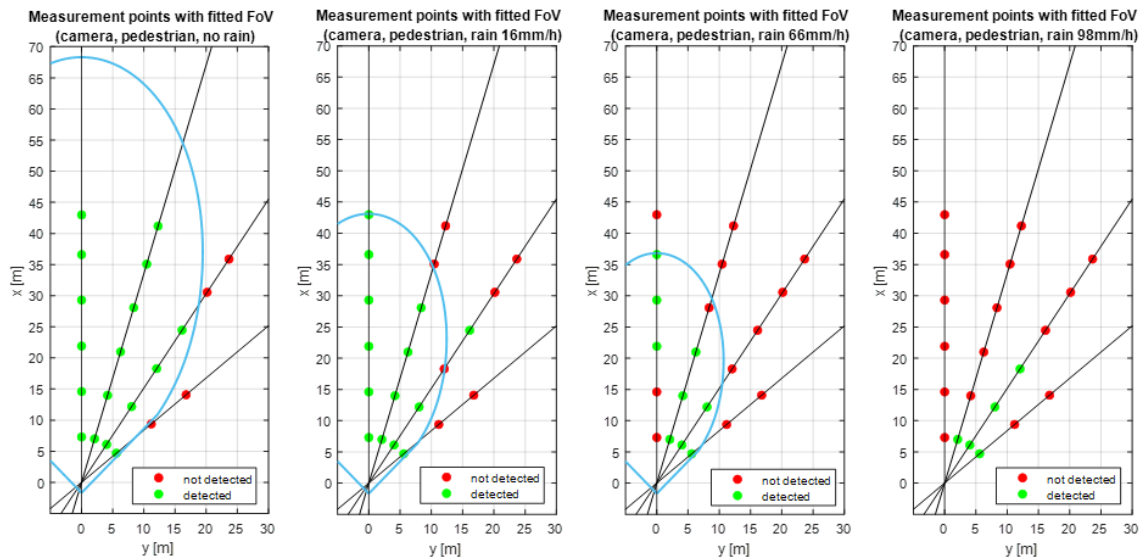


Figure 22: Measured points and corresponding camera detections for the pedestrian target under rainy conditions with fitted theoretical FoVs.

4.2.3 Results summary, limitations & outlook

This section gives a summary of the evaluation results and the limitations of this approach and an outlook on future work.

4.2.3.1 Summary of the results

With the data of the second measurement campaign and theoretical characteristics of the investigated radar and video sensor, FoVs were generated for the pedestrian target and different rain intensities. The resulting FoVs can be integrated into simulations to estimate the influence of different weather conditions and give an indication of how far today's sensors already cover their effective field under adverse weather conditions.

In Figure 23 the resulting FoVs are shown overlaid for dry conditions and the tested rain intensities to highlight the difference. Considering that 16mm/h is already an extremely high rain intensity according to Deliverable 2.6 (SAFE-UP, Deliverable report D2.6, 2021), the conclusion can be drawn that the radar is solely slightly impaired by rain, especially by common rain intensities. The effect is higher with the camera, but it can still robustly detect pedestrians within a restricted FoV for 16mm/h.



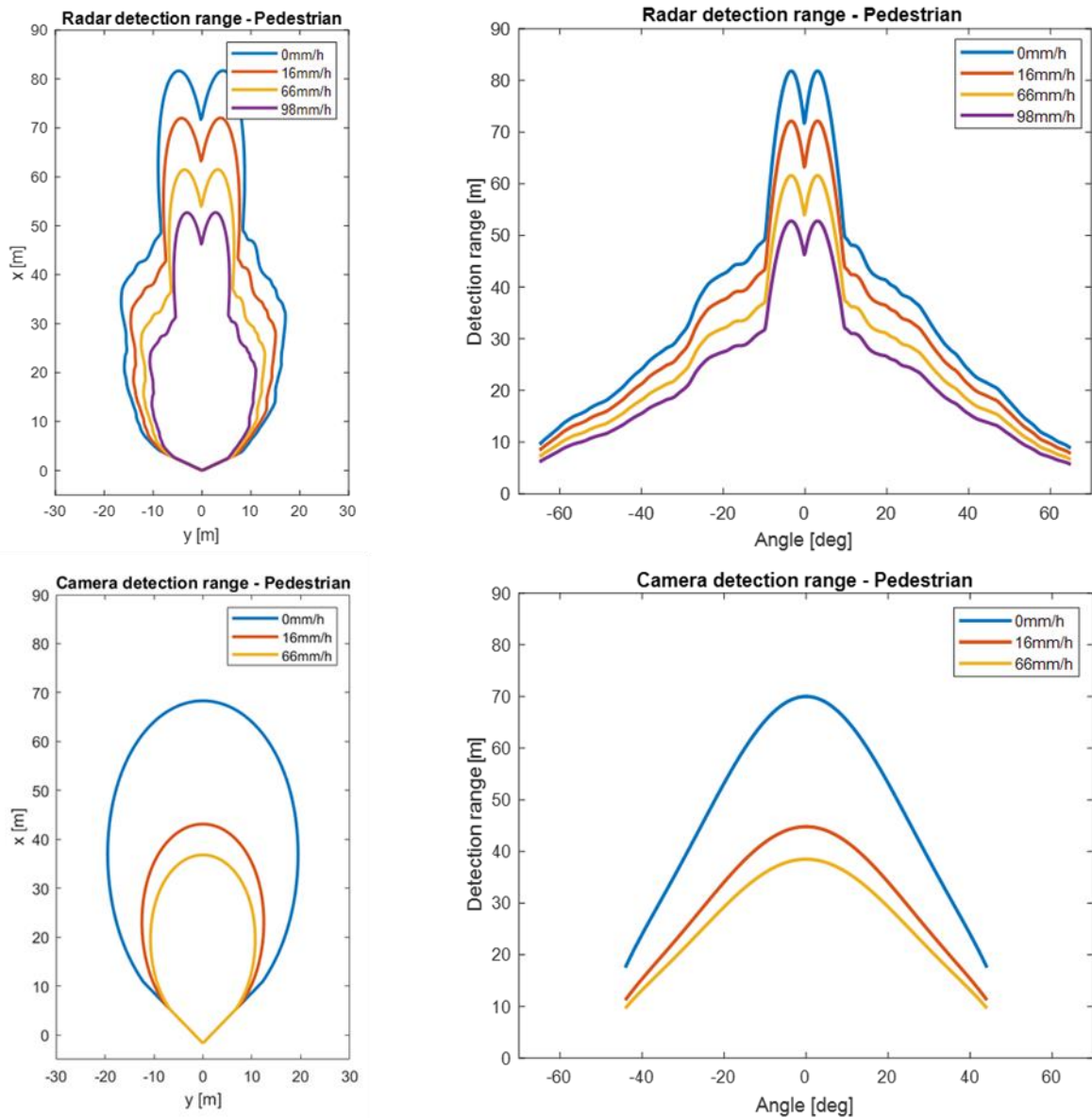


Figure 23: Summary of the results for the investigated radar (top) and video (bottom) sensor at dry and rainy conditions in Cartesian coordinates (left) and polar coordinates (right)

The detection performance of the sensors, both from the radar sensor and from the camera, is sometimes severely limited compared to the theoretical limits. This is partly due to the test setup in the hall. However, there are also limitations that stem from the sensor technology itself, which are described in the following.



This project has received funding from the European Union's Horizon 2020 research and innovation programme under Grant Agreement 861570.

4.2.3.2 Limitations

Limitations of testing in the test hall

Due to the limited rain area in the hall, for the complete determination of the sensor FoVs an estimation can only be made by theoretical assumptions. On the one hand the limitations refer to the range, on the other hand to the aperture angle.

Another problem arises from the rotation of the vehicle. The vehicle must be either turned such that the sensor points into the barrier or into the open hall. In both options, reflections from walls and edges can create ghost objects that have to be filtered even though measures have been taken to absorb metallic objects and edges.

The rain intensities in the test hall can be classified as extremely high with regard to the intensities that are normally encountered in European regions. The testable rain intensity range in the hall is from a minimum of 16mm/h to a maximum of 98mm/h. However, a lower rain intensity would be desirable as 16mm/h is already significantly above the threshold of 10mm/h set for heavy rain by the German weather service DWD. Moreover, in a crash event including VRUs, the rain intensity is usually significantly lower as shown in Table 7 from (SAFE-UP, Deliverable report D2.6, 2021). In addition, high rainfall intensities entail a high test effort, since the water must be removed again after a few test runs.

| Rain intensity (i) label | Range by DWD [mm/h] | Median in GIDAS crashes [mm/h] | Mean in GIDAS crashes [mm/h] | 90 th percentile in GIDAS crashes [mm/h] |
|--------------------------|---------------------|--------------------------------|------------------------------|---|
| Light | $i < 2.5$ | 0.54 | 0.87 | 1.7 |
| Moderate | $2.5 \leq i < 10$ | 0.96 | 2.7 | 3.6 |
| Heavy | $i \geq 10$ | 1.1 | 3.1 | 5.7 |

Table 7: Comparison of the extracted values of the GIDAS to the ranges defined by the German weather service DWD for the intensity labels. Table from (SAFE-UP, Deliverable report D2.6, 2021)

Difficulty of exact vehicle positioning

Another challenge regarding the positioning is the accuracy of the angular rotation of the vehicle. This could theoretically be achieved with a dGPS system, but this is only limited possible inside the hall due to a lack of GPS reception and would require separate measures. Practically, the manual positioning of the vehicle with an accuracy of less than one degree is difficult to implement. Therefore, as described in section 4.2.1.2 a correction of target position must be performed, when the data shows systematic errors.



Static testing

One of the biggest influencing factors for the object detection are the algorithms for object formation. As described in the following, the radar sensor as well as the camera have limitations in static tests.

The radar sensor has a negative property in static tests, because it can hardly distinguish static objects from reflections on the ground or other objects. A moving object can be detected in a much more stable way by means of the Doppler effect. Therefore, it is also important that at least the pedestrian's legs are moving. For the bicycle target the rotations of the tires are missing.

There are also limitations for static object detection with a camera. First, the static position of the test vehicle has a negative effect on the distance estimation to the object. The calculation of the distances is also dependent on the ego motion and the horizon formation, which is limited in the hall. Secondly, the algorithms are trained for realistic movements of the VRU objects and not for objects in rigid positions. These limitations in these static tests can lead to a loss of performance especially with the camera. For example, the pedestrian target with moving legs is a non-realistic form of movement of a pedestrian and can cause implausibilities. Similarly, the stationary standing bicyclist can lead to incorrect distance estimations, since the legs are not on the ground.

It can therefore be assumed that the detection performance is higher with real dynamic objects than with the static tests in a hall. This finding must be taken into account, when using the given FoVs.

Another effect of static testing, which has not yet been further investigated, is caused by the static execution in rainy conditions. A higher speed means that the rain does not fall exactly perpendicular from the vehicle's perspective, but also towards the vehicle and thus towards the camera and the radar sensor.

Object orientation

Due to the high testing effort in the hall under the described limitations, solely one rotation of the objects was tested, which is representative for crossing objects. To obtain a complete sensor model, it is necessary to investigate also the rotation of the objects under different boundary conditions. The pedestrian can be assumed to be a cylindrical object due to its extension and the detection performance can be considered to be similar from all sides. However, for the bicycle and motorcycle further measurements would be necessary.

Sensor and algorithm dependency

The results of the second measurement evaluation shown in this deliverable depend on the used sensor as well as the algorithms. For new sensors algorithms the tests would need to be re-executed.



4.2.3.3 Outlook

The goal of the second measurement campaign was to generate FoVs for the radar and the video sensor so that the results can be integrated into simulations and trajectory viewers to estimate the influence of different weather conditions and give an indication of how far today's sensors already cover their effective field under adverse weather conditions.

Therefore, scenarios from (SAFE-UP, Deliverable report D2.6, 2021) for pedestrian accidents will be simulated with and without rain influence as well as with and without function intervention. The rain influence will be modelled by adapting the FoVs as described in this deliverable and by adjusting the friction coefficient. The methodology and the results thereof will be part of the Deliverable D3.6 of the SAFE-UP project.

Using the pre-crash matrix as part of the GIDAS database, the movements of participants involved in the pre-accident phase up to the crash can be displayed. The trajectories in relative and absolute representations for all conflicts are analyzed in Deliverable D2.6. (SAFE-UP, Deliverable report D2.6, 2021).

- 298 Pedestrians, all injury severities, GIDAS-PCM, 2020-1

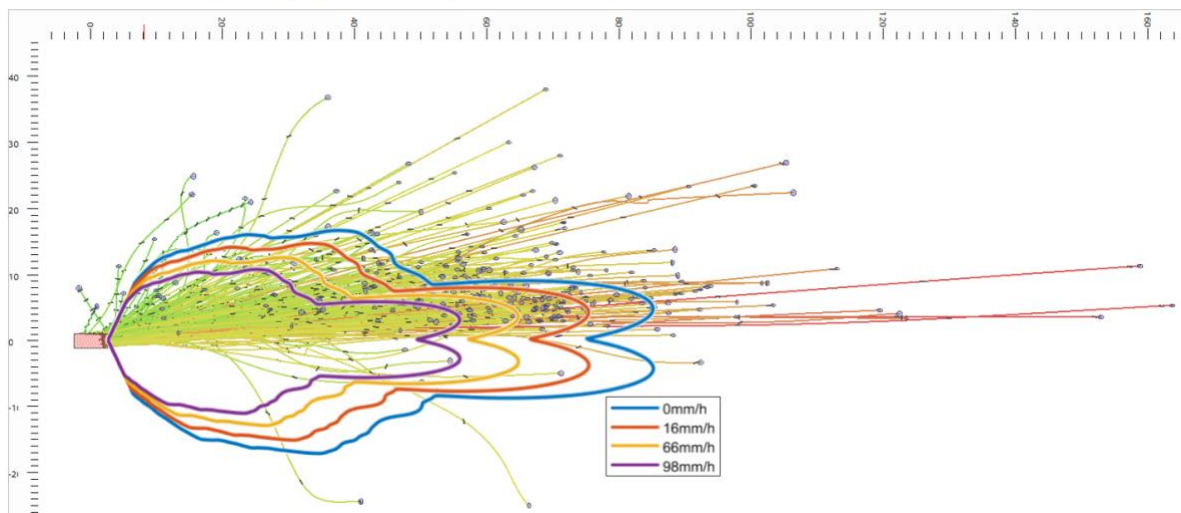


Figure 24: Crossing from left without sight obstruction (CLwoSO) – Trajectories, relative and Radar FoV for different rain levels

Figure 24 shows the relative approach of crossing pedestrians (n=298 pedestrians in GIDAS PCM as of January 2020) from the left with no obstruction (CLwoSO) to the view of the car in the time range from Time-To-Collision = 5 seconds to Time-To-Collision = 0 seconds. With 19.5% of the seriously injured/killed pedestrians, this scenario is a focal point in accidents. The proportion of accidents at night and in the rain is comparatively higher within this scenario. In addition to that, Figure 24 shows Radars Field of View for different rain levels. The evaluations for the restriction of the Field of View for radar and camera can now be used in TRAVIS (AUDI Tool “Trajectory Analysis and Visualization”) in combination with the



approach trajectories and - as visualized in the Figure 24 - visualize the restriction of the Field of View. Furthermore, using TRAVIS it is possible to evaluate the time delay (measured as time-to-collision) that occurs before pedestrians are in the field of view of the sensor as precipitation increases. The methodology and the results thereof will be part of the Deliverable D3.6 of the SAFE-UP project.

4.3 Results of the fourth measurement campaign

4.3.1 Evaluation LiDAR sensors

4.3.1.1 Short Range LiDAR

The boundary conditions are

- measurement was performed in a static environment
- distance to the static targets is 15 meters

To briefly state, the dimension of 10 % reflectivity Lambertian target is 2x2 meters, RA3 target is 1x1 meters and RA2 covers an area of less than 1 m². The theoretically possible maximum number of measured points from a target is given by $N_{\text{theo}} = \frac{\Delta\phi}{h_{\text{res}}} \cdot \frac{\Delta\theta}{v_{\text{res}}}$, where $\Delta\phi$ and $\Delta\theta$ are the azimuthal and elevation opening angles of the targets extensions relative to the LiDAR mounting point and h_{res} and v_{res} are the horizontal and vertical angular resolution of the LiDAR.

Detection probability:

The detection probability DP is defined as ratio of theoretical maximum points on target to measured number of points N_{meas} on the target: $DP = \frac{N_{\text{theo}}}{N_{\text{meas}}} = \frac{\frac{\Delta\phi}{h_{\text{res}}} \cdot \frac{\Delta\theta}{v_{\text{res}}}}{N_{\text{meas}}}$.

For dry conditions, the detection probability of all the targets are close to 1. There could be a small difference in value due to the theoretical point cloud calculation taken from corner-to-corner along all edges and this do not have to necessarily match the real-time capture of point cloud data on target due to a lot of reasons such weather, optics, etc.

Point Cloud Data Analysis:

The Hesai QT128 – Short Range LiDAR sensor was tested under the different environmental conditions mentioned above.

Target Visibility and Detection Probability:

Figure 25 shows the target visibility as the number of points reflected by each target under different environmental conditions. Figure 26 shows the detection probability.

Starting with Lambertian target of 10% reflectivity in dry conditions, 100% reflectivity of target is observed. In heavy fog of 10 meter visibility, the target is completely lost due to absorption and scattering phenomena of Laser beam in fog. No points were detected on the target in this



weather condition. In Rain with 32mm/h of intensity, the detection probability of the target has dropped from 100% to 60%.

For RA3 target, all points on target are detected giving 100% detection probability in dry conditions. In heavy fog of 10m visibility, the target is no more fully visible. However, compared to the Lambertian and RA2 target, the detection probability is higher. The detection probability has reduced only by 0.3 giving it 70.45% detection in Fog. In rain of 32mm/h, a similar trend is observed where the detection probability of RA3 is higher than the other targets. In terms of value, the detection probability of RA3 is 95% which is higher than RA2 by 15% and by 35% with Lambertian target.

For the RA2 target, in dry condition the detection probability is 100%. The resolution of the sensor is less in longer distance, and this is evident from the less points on the target even in the best condition. The detection probability is 100%. In Fog, with 10m visibility range the number of points on the target is reduced significantly. The detection probability is reduced from 100% to 25% and this is due to the attenuation in fog. The third weather condition is 32 mm/hr of rain intensity. In Rain, RA2 target is well visible compared to Fog and detection probability stays at 80%. This phenomenon supports the reflectivity behavior of the RA2 target.

The analysis shows that for different targets, the number of points in dry condition is higher than in rain and fog conditions. Both fog and rain reduce laser intensity by absorption and scattering phenomena of the Laser beam by the water droplets. The Bar graph helps to outline the scenario from statistical point in terms of number of points on each target for different weather conditions to derive target visibility and detection probability.

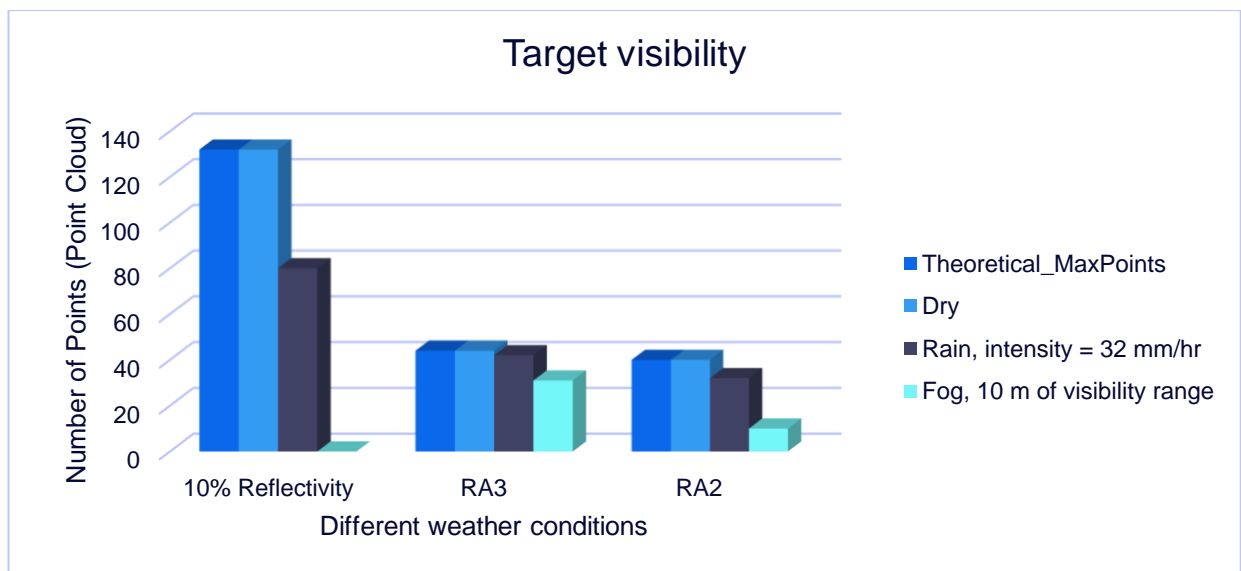


Figure 25: Target visibility



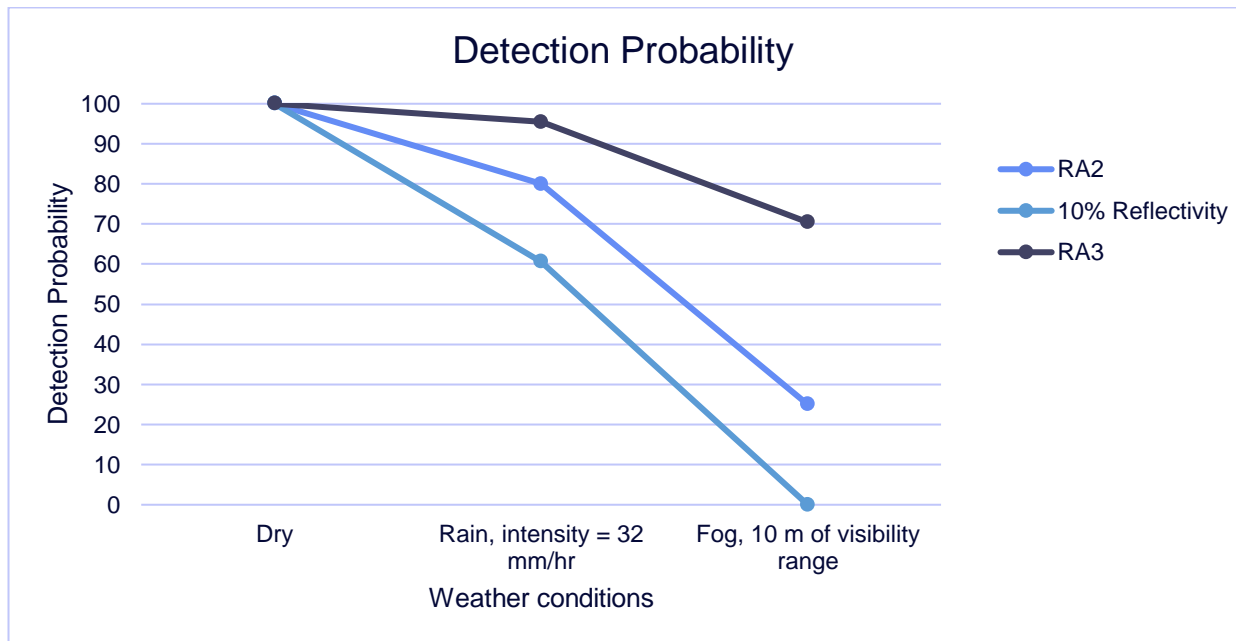


Figure 26: Detection probability

4.3.1.2 Long Range LiDAR

Rain

For the use of LiDAR data in an automotive context the intensity information of the objects is often used to distinguish between different kind of objects.

In the following section, the influences of rain on the intensity and detection probability of a Long Range LiDAR are considered.

Figure 27 shows the normalized intensity for different rain rates. The yellow bars show that the normalized intensity of the retroreflective RA3 target is constantly 1 in overall measurement across different rain rates. The constant intensity of the retroreflector target shows that the sensor is always in saturation due to the highly reflective properties of the target.

The normalized intensity of the Lambertian 10 % target, indicated by the blue bars, shows a significant drop by 74 % from an initial 0.62 in no rain condition to 0.16 at a rain rate of 82 mm/h.

This is in contrast to the retroreflector target where the intensity of the Lambertian target is at least 38 % lower due to its optical properties.

The decreasing trend of the intensity over the rain rates can be attributed to the scattering, refraction and absorption of the laser pulse due to the raindrops in the air.



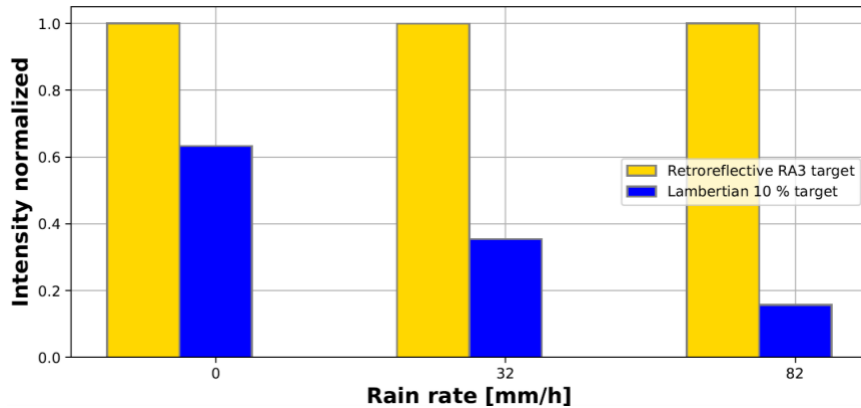


Figure 27: Intensity analysis for a rain environment

Figure 28 shows the detection probability (DP) for the rain rate considered. The blue bars of the Lambertian target shows a decrease of the detection probability with increasing rain rate. The 58 % decrease in the detection probability at a rain rate of 82mm/h indicates a significant object detection loss.

The yellow bars shows that the detection probability for the retroreflective target is 100 % without rain and at a rain rate of 82 mm/h. Whereas at 32 mm/h, the detection probability drops to 59 %. From the analysis, it can be understood that all points of target are detected even in 82 mm/h. The drop in detection probability at 32 mm/h can be attributed to inhomogeneities of the rain inside the measurement hall.

During point cloud analysis, it was observed that raindrops also form as objects ahead of actual targets affecting the detection probability.

This is supported by the normalized intensity value of 1 from Figure 27, which indicates that no points are lost due to low intensity.

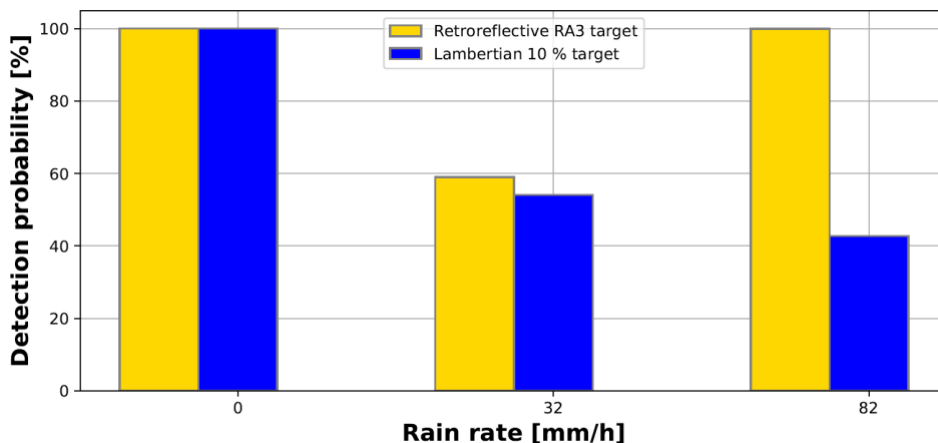


Figure 28: Detection probability analysis for a rain environment



Fog

In accordance with the previous evaluation, the influences of fog on the Long Range LiDAR are considered here.

Figure 29 shows the normalized intensity for fog in different densities. The yellow dots show a steep increase of the normalized intensity from 0 % at 16 m to 84 % at 21 m. This is followed by less steep slope approaching the intensity saturation of 97 % at 101 m visibility of the retroreflective RA3 target.

The Lambertian 10 % target, indicated by the blue dots and referring to the right scale, show only a very small, normalized intensity value between 0.027 and 0.032. The intensity values can be observed from 33 m.

Comparing the two targets it shows that normalized intensity of the retroreflective target is around 28 times larger than the Lambertian target.

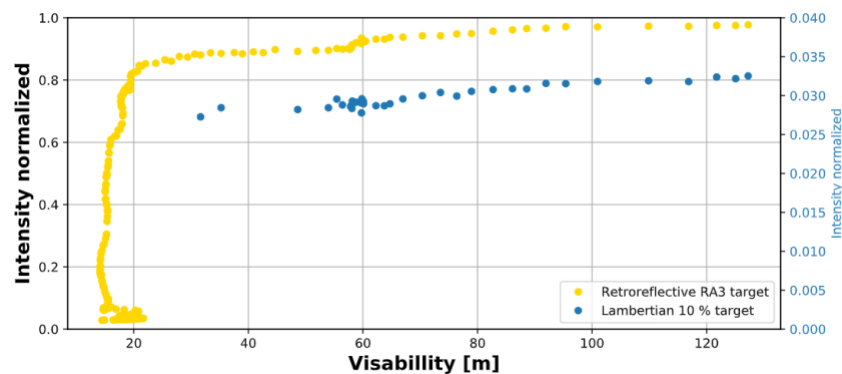


Figure 29: Intensity analysis for a fog environment

Figure 9 shows the detection probability for the different fog densities.

The yellow dots shows the detection probability of the retroreflective target at 21 m to be around 100 %. Within 16 m to 21 m visibility, all points range between 0 % and 100 % detection probability. The reason for the distribution of these points could be found in some jittering data of the reference sensor at that given range.

For the blue dots of Lambertian target the detection probability starts to increase at a visibility of 57 m and increases to a maximum of 15 % at 124 m.

From the chart it can be derived that the retroreflective target can be much more reliable and also in lower visibilities detected than the Lambertian target.



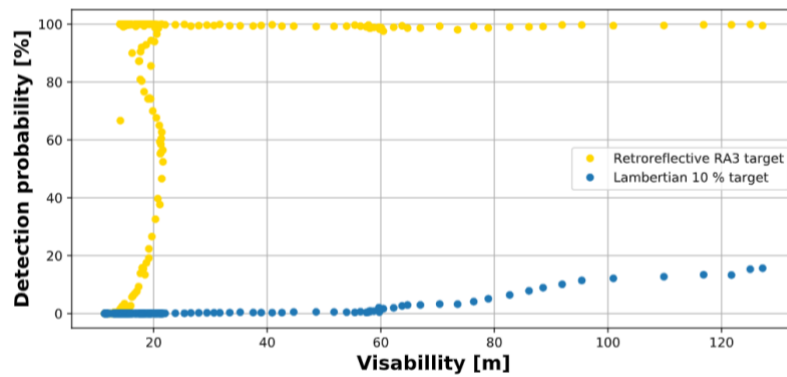


Figure 30: Detection probability analysis for a fog environment

4.3.1.1 Evaluation of Wiper Cleaning System

A mechanical wiper cleaning system is mounted on top of the Long Range LiDAR for cover glass cleaning in extreme weather conditions. The evaluation is done to analyse the effect of wiping system on the LiDAR performance during rain. Therefore a qualitative analysis comparison on area of target during dry, in 32 mm rain with and without wiping given the cleaning system is a development prototype. The Figure 31 shows the effect of cleaning system. In Dry weather, maximum number of points are obtained and considered as reference. For RA3 target in yellow bar, at a rain intensity of 32 mm per hour, without wiper system at a standstill condition the effective area of target reduces by 17.3% . But with the continuous wiping of LiDAR cover glass, the effective area reduces only by 3.5% from reference (Dry condition). Similarly for other targets, the effective area of target without wiping system is reduced by 36% for RA2 (Stop Sign) and by 55% for Lambertian target (10% reflectance). On the other hand, with continuous wiping, the effective target area is reduced by 14.7% for RA2 and 32.7 % for Lambertian target (10% reflectance).



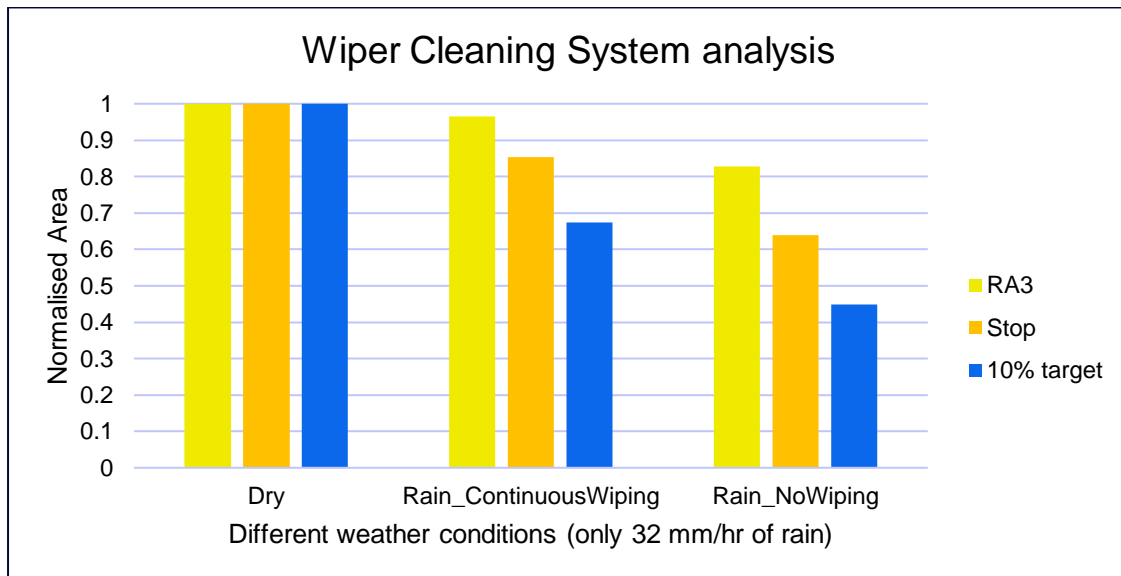


Figure 31: Effects of the wiper cleaning system

4.3.1.2 Conclusion

Long Range LiDAR

If you compare the influences of rain and fog it can be observed that for the low reflective Lambertian target fog has a much bigger influence on the performance than even extreme rain rates. For the retroreflective target only very dense fog degrade the performance in the given evaluations due to the high reflectivity which lead to saturation effects.

It could be shown that the optical properties of the targets are a key factor in object detection.

Short Range LiDAR

In summary for short range lidar, the detection probability of different targets reduce significantly in bad weather conditions.

Wiper based cleaning system

The above analysis is only an initial proof of concept to understand the effect of wiper based cleaning system and also test the working of such cleaning system. The analysis shows that wiper based cover glass cleaning system has an good effect in terms of achieving a better point cloud compare to without a cleaning system. As stated before, the results are confined to only testing of proof of concept and not a comprehensive evaluation.



4.3.2 Evaluation Fog sensor

For the description of the mounted fog sensor and road condition sensor on the vehicle see section 2. While the latter device is produced for the usage in vehicles, the fog sensor is typically used in a stationary setup like the runway of an airport. Thus, one goal of the measurement campaign is to verify whether the fog sensor also works while the vehicle is driving.

Fog manifests as a contrast reduction which is best modelled by an exponential attenuation over distance and an atmospheric attenuation coefficient β , also called extinction coefficient. By means of the extinction coefficient the visibility range is defined as the maximal distance from an observer to an object, still being distinguishable from the background.

The utilized fog sensor is a transmissometer. It determines the ratio of emitted to received light. Therefore, laser light of a certain wavelength is emitted into a predefined volume where it scatters forward into a photodetector. For the given distance from the emitter to the receiver the attenuation coefficient β is calculated. Strictly speaking, the determined attenuation coefficient is only valid within the predefined volume and thus the same holds for the derived visibility range. However, under the assumption of homogeneous fog the result can be considered valid in the vicinity of the fog sensor.

The aim of the following measurement is to validate the functionality of the fog sensor Campbell CS125 which is mounted on the vehicle and is expected to work while driving. To this end we compare the measured visibility range to the results of the stationary device within the weather hall. The latter is a fog sensor, Sick Visic620 (SICK, 2022) of identical measurement principle. Since the assumption of homogeneity of fog is only valid within a limited part of the test track, the test vehicle is only driving laps within that restricted region. While driving laps the measurement vehicle passes the stationary fog sensor. This experimental design compromises two goals: First, to compare the fog sensors under the assumption of homogeneous fog. Second, to verify the viability of the fog sensor while driving.

The result of the comparison is shown in Figure 32 where measurements of the reference sensor (SICK) are displayed in blue, and the sensor mounted on the test vehicle is depicted in orange. Once the fog production starts the Sick sensor reports a sudden decrease of the visibility range. This contrasts with the Campbell sensor showing a much slower decay in the visibility range.



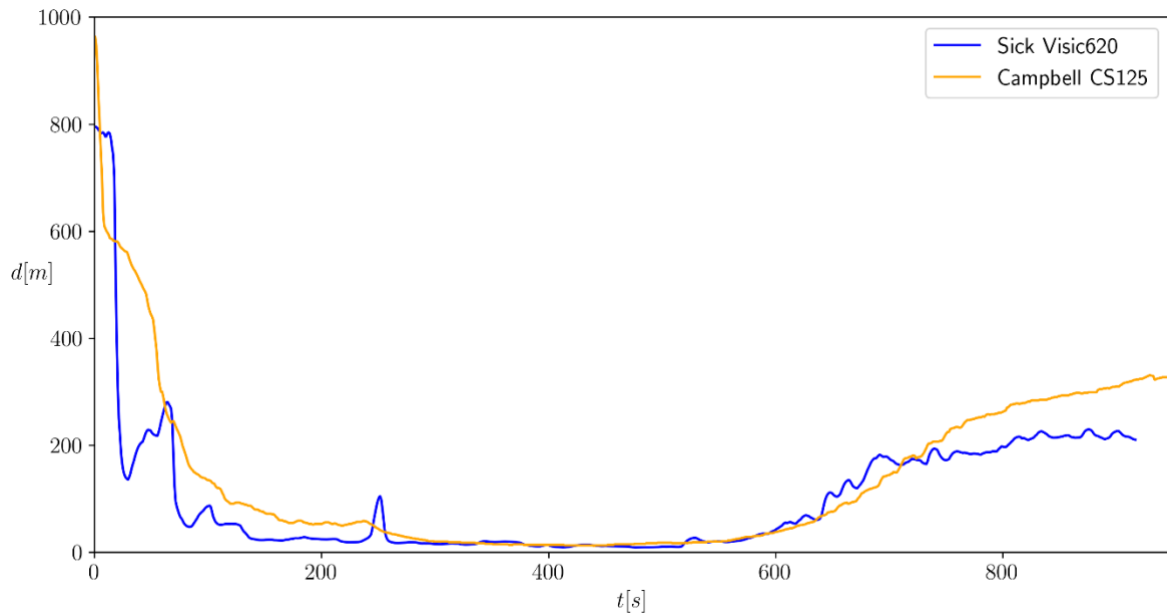


Figure 32: Comparison of the measured visibility range of two fog sensors. The result of the stationary device Sick Visic620 is shown as blue curve. For the mobile sensor mounted on the vehicle Campbell CS125 the result is shown in orange.

For a sufficiently long period of time dense fog nearly distributes homogeneously inside the weather hall. Both fog sensor measure visibilities ranges in the same interval of [11m – 15m], see e.g., for $t=400$. After fog production is stopped the visibility range slowly increases again, which is captured by both devices.

The measurements displayed in Figure 32 show that both fog sensors provide similar results. Stronger fluctuations for the Sick device might result from shorter configured average times but could also be due to a lower number of internal measurements (per second, frequency). For a systematic study of the observed deviations of the visibility range further experiments are necessary which were out of scope for this campaign.

More importantly, it shows that the Campbell sensor is capable to measure the visibility range while driving, verifying the viability. Despite possible influences like the airflow/turbulences of the car or vibrations, the sensors provide comparable results. However, the vehicle speed during the experiment was relatively slow only up to 15 km/h as the homogeneous region of fog and the dimensions of the weather hall is limited. This needs to be further analyzed during real-world foggy weather, e.g., on a test track.

4.3.3 Evaluation Road condition sensor

Adverse weather conditions not only deteriorate visual perception but also lead to drastically change of the physical properties of the road surface. Rain, snow and ice decrease the friction coefficient and thus to less adhesion between the road surface and the vehicle, leading to



reduced driving quality and safety. In order to record these effects during the recording campaigns, it is planned to utilize the road condition sensor Vaisala MD30 for generating associated ground truth data.

Therefore, one of the aims of the measurement campaign in the weather hall is to assess the sensor functionality. With a laser the road condition sensor tracks the road surface and measures various quantities like the thickness of rain, snow or ice layer and the surface temperature. By aggregating these measurements, the sensor also provides a derived output of the road surfaces state. We take advantage of the synthetic rain, produced on one side of the test track inside the weather hall.

The result of such a drive test is shown in Figure 33. The surface state is shown in a) which is subdivided into the three categories dry, moist and wet. In c) the thickness of the water layer is shown in units of millimeters. Initially the car is positioned in a dry part on the test track where no water is on the surface. Driving the car through the artificial rain of 32mm/h two regimes can be identified. First, an intermediate regime where the surface is moist and only a very thin layer of water with approximately 0.05 mm is recorded. Second, a regime where the surface is wet and a thicker layer of water of approximately 0.75 mm is measured. The first regime is due to water spray moistened parts of the test track not covered by larger drops. This is shown in (b) where the car approaches the watered part of the test track. Eventually, the second regime is within the almost homogeneous rain on the test track shown in (d). After passing the rained part of the test track, the surface state is again considered to be dry, shown in (f).

The results indicate that the sensor can record the current state of the road surface. Note that further measurements must be performed in the winter period in order to validate the snow and ice layer thickness and make use of other quantities like the road temperature. This, however, was out of scope here.

Like fog also rain leads to a decrease of the visibility range. We thus evaluate in addition the visibility measured by the fog sensor Campbell CS125, shown in (e). Initially the visibility range is not limited and measured with approximately 17000 m. After the artificial rain is turned on and the car is driving through the rain the visibility range decreases rapidly. The recorded visibility range, however, is not increasing instantly after reaching the end of watered part of the test track.

Eventually, we find that the fog sensor also detects rain scenarios, however the provided visibility ranges are questionable. Nevertheless, the fog sensor might act as an additional trigger and give a rough indication of the real visibility range.



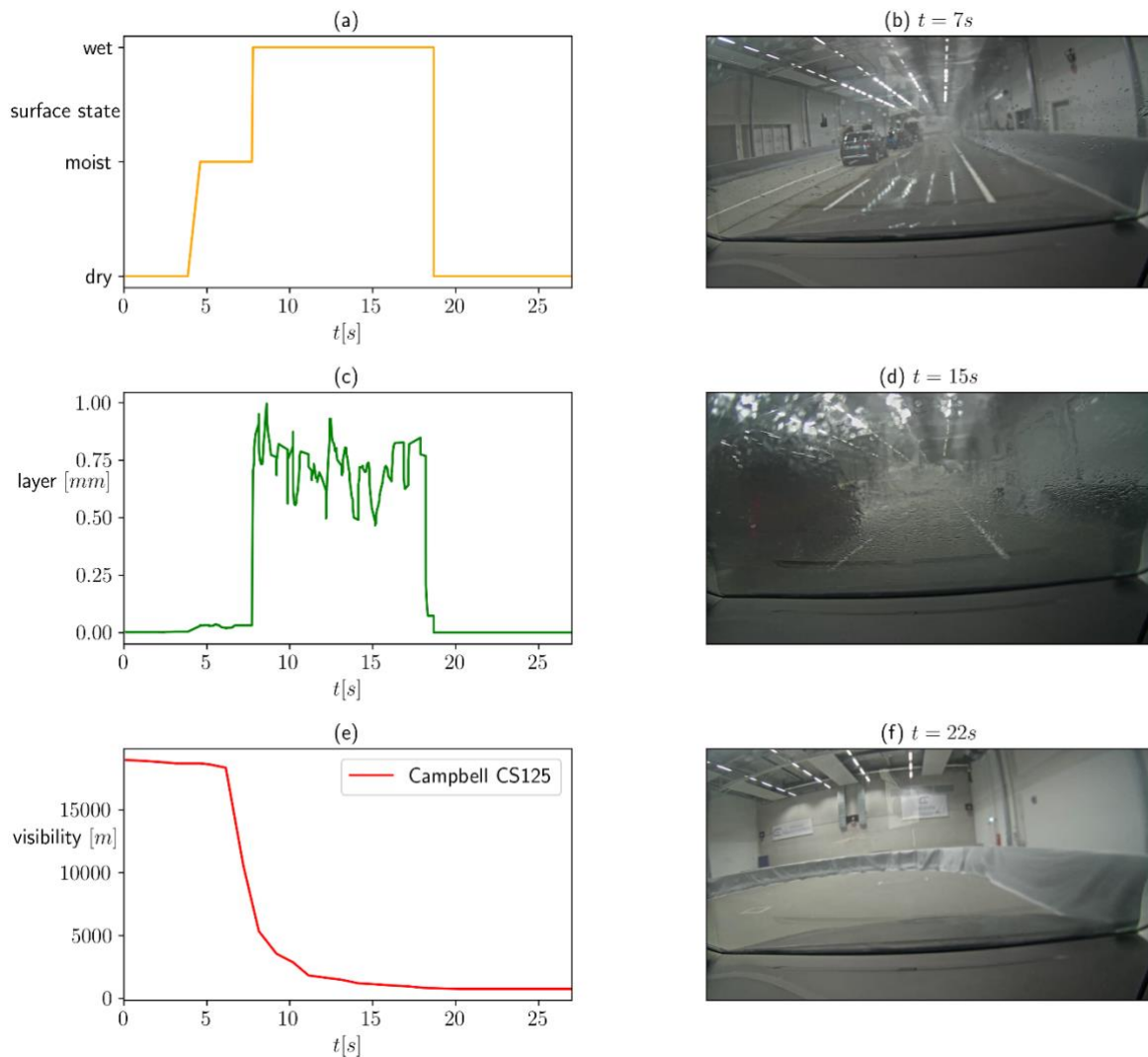


Figure 33: Comparison of results of the road condition sensor and images during measurement campaign. The panels show (a) the surface state, (b) water layer thickness and (c) visibility range.

To summarize, both sensors can provide ground truth data in adverse weather conditions. Mounting them on vehicles of the recording fleet enables to annotate data and thus identify adverse conditions in large data sets. These allow for the development of more robust CNNs increasing functional safety in future applications.

4.4 Weather filter

The overall scope of the weather filter is to bring weather effects on automated vehicles (AVs) into simulation to accelerate testing and validation with the focus on novel active safety systems for AVs. As described in the previous deliverable D3.2 the idea is to come from a physical approach purely based on equations that models primary effects such as attenuation



in order to change sensor related parameters quickly without the need of extensive measurement campaigns. Therefore, a hybrid approach was chosen that is based on the physical approach but adapted in order to match the actual measurement results which contain all sorts of primary and secondary effects such as water on the sensor lens among others. This Chapter includes elements and summaries of the Deliverable reports D3.2 (SAFE-UP, Deliverable report D3.2, 2021) and D2.10 (SAFE-UP, Deliverable report D2.10, 2022) including the latest results.

Figure 34 shows the concept of individual sensor filters on object level between the ground truth of the simulation and the input of the motion planning algorithms which contain the active safety algorithms.

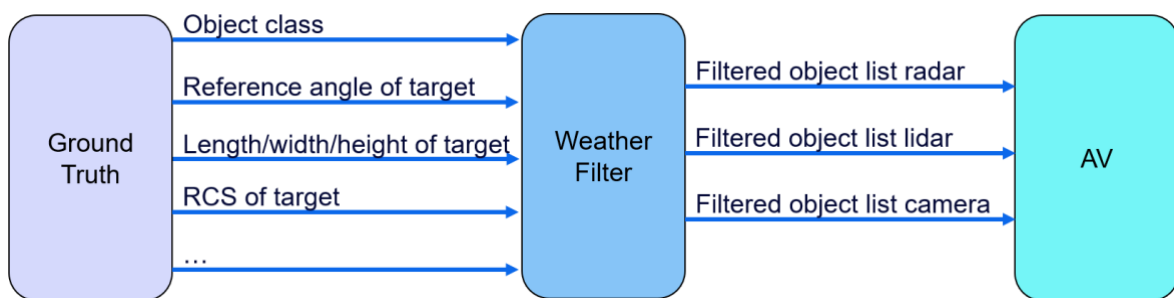


Figure 34: Weather filter implementation within the given software framework

Tuning parameters for the weather filter during runtime are rain rate [mm/h], the visibility in fog [m], and the temperature [°C]. Other environmental conditions such as fog or rain type can be changed beforehand if required. However, all results in the following are based on measurements within the CARISSMA testing facility for continental fog and rain.

Note that the visual range under fog is used as an intuitive measure for better understanding. The weather filter itself is purely based on physics, so that the visible range needs to be extracted and converted according to Figure 35.



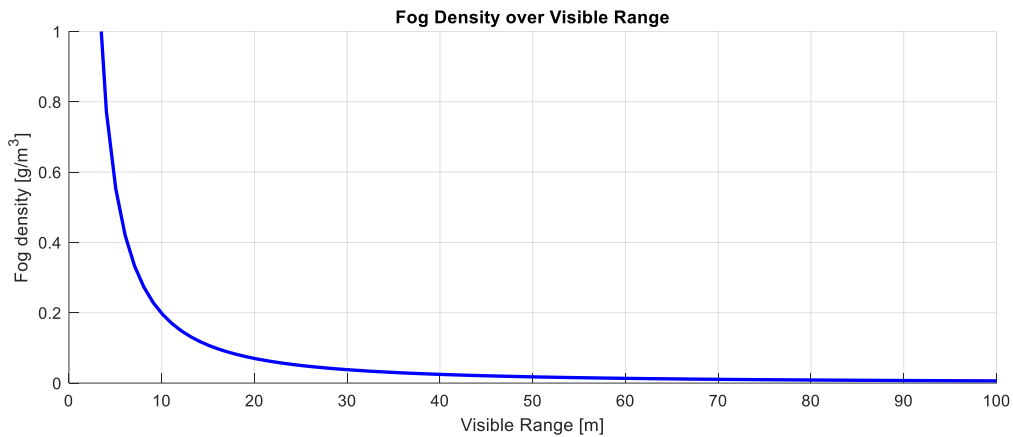


Figure 35: Dependency between fog density and visible range (SAFE-UP, Deliverable report D2.10, 2022)

As derived and described in the Deliverable report D2.10 (SAFE-UP, Deliverable report D2.10, 2022) the main outcomes of attenuation for lidar and radar based on the hybrid weather filter approach are Figure 36 and Figure 37.

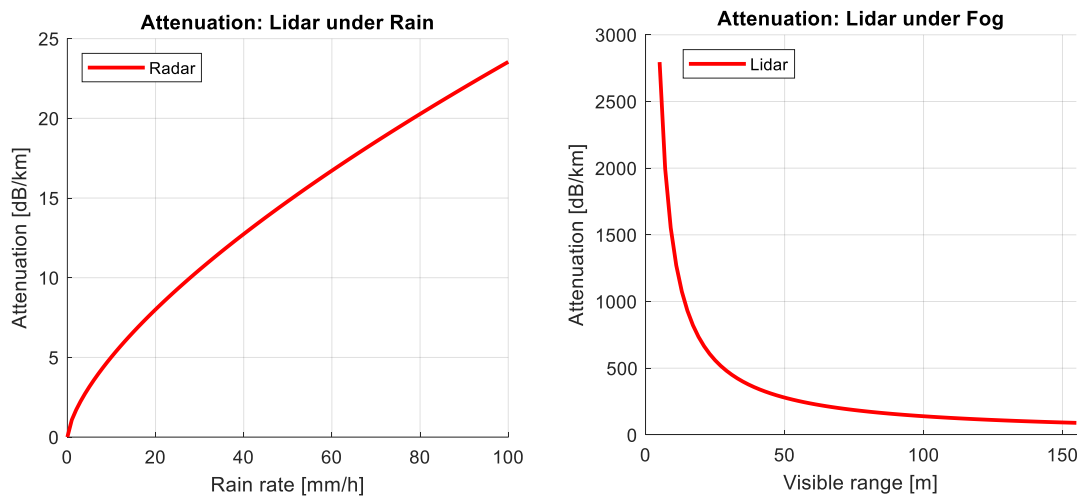


Figure 36: Lidar attenuation dependency on rain and fog (SAFE-UP, Deliverable report D2.10, 2022)



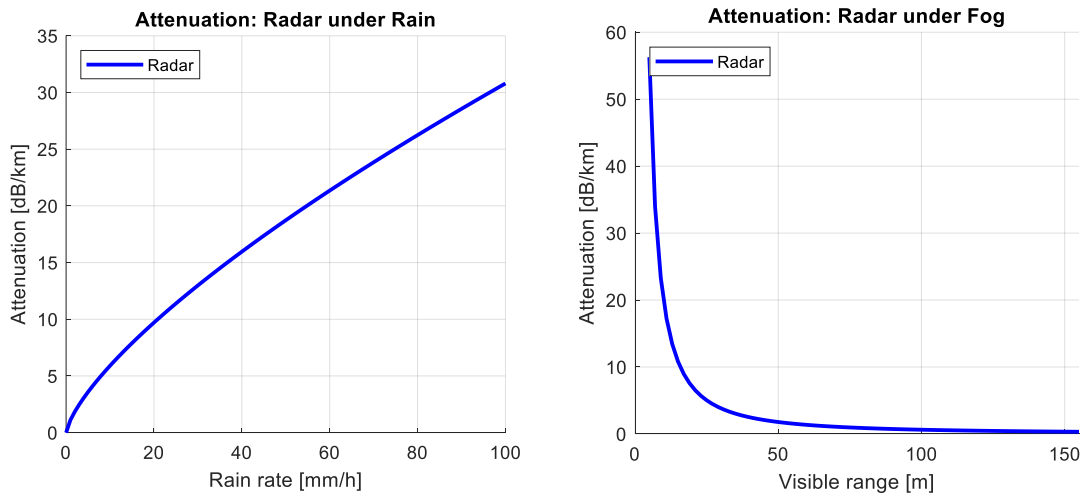


Figure 37: Radar attenuation dependency on rain and fog (SAFE-UP, Deliverable report D2.10, 2022)

Both figures show the expected behavior after the calibration of the physical approach to include secondary effects. The attenuation and the trend of both sensors is similar under rain even though the lidar suffers more from the rain in terms of attenuation. A higher difference can be seen by comparing both sensors under fog where the purely optical sensor suffers under its non ideal wave length (850 μm) compared to the radar's wave length of 3,89 mm.

According to Figure 38, the camera suffers even more under rain conditions being an optical sensor without an active light source. An investigation of the attenuation over fog was not required for the camera because of the assumption that the visible range equals the detection range of a camera.



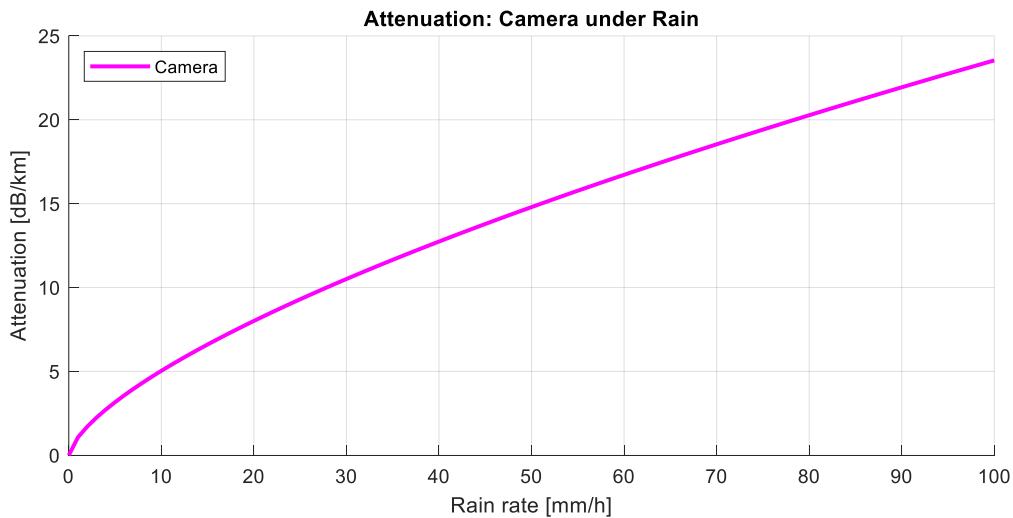


Figure 38: Camera attenuation for different rain conditions (SAFE-UP, Deliverable report D2.10, 2022)

The resulting maximum detection distances are presented from Figure 39 up to Figure 44. Figure 39 shows the detection thresholds for the maximum detection distance under the rain conditions defined for the weather filter. For the described case of a target rotated by 0°, the detection of the pedestrian is possible over longer distances compared to the detection range for the cyclist. In particular, the radar cross-section (RCS) confirms this fact, although highly reflective surfaces such as the license plate of a PTW are not considered here. It is expected that these detection ranges will change significantly when the targets are rotated around their z-axis defined as the axis from bottom to top in the center of gravity for the standing vehicle.

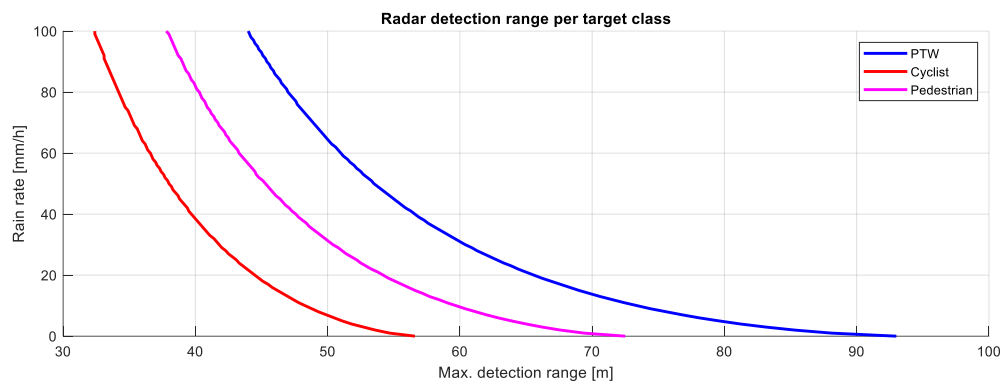


Figure 39: Detection thresholds per target class for radar under rain (SAFE-UP, Deliverable report D2.10, 2022)

Similar to the detection thresholds under rain, is the distribution for different visibility ranges in fog (Figure 40). It can be seen that the radar hardly loses range up to about 100 m of



visibility, and only below about 50 m of visibility, a drastic drop in the range is seen for all target classes.

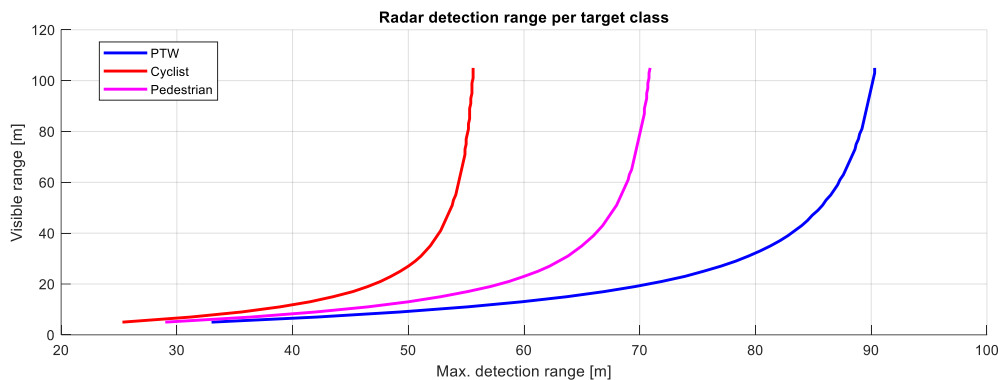


Figure 40: Detection thresholds per target class for radar under fog

The associated detection thresholds for lidar under different rain conditions is illustrated in Figure 41 and shows a generally higher sensitivity in rain compared to the radar sensor.

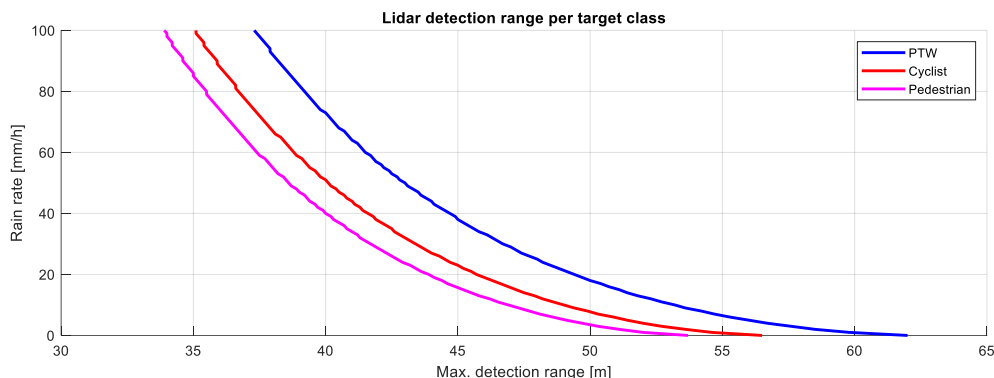


Figure 41: Detection thresholds per target class for lidar under rain

The influence of fog on the lidar sensor (Figure 42) is considerable based on the detection thresholds, which means that only limited functionality is guaranteed in real operation. Also, the visible area of the target becomes less relevant with increasing fog density.



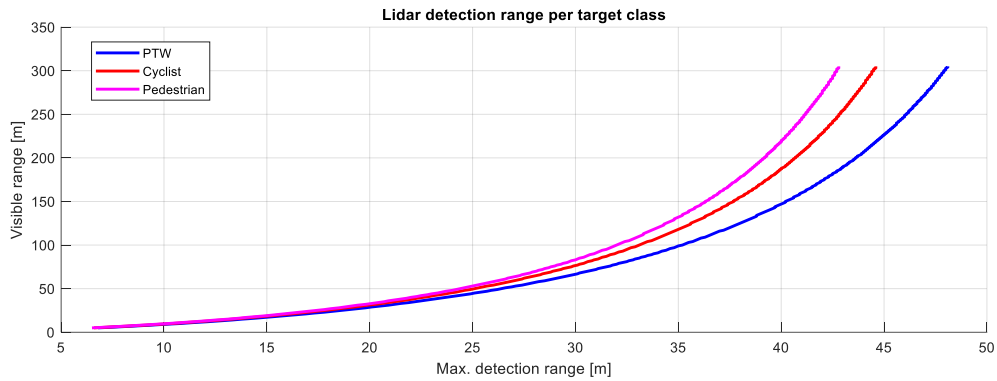


Figure 42: Detection thresholds per target class for lidar under fog

Since the evaluation of the camera at the object level is strongly dependent on the perception, which is not available, the results of the camera are mainly based on the physical approach. As with lidar, secondary effects have a marginal impact on the detection range, such as water on the windshield (with corresponding cameras behind it). With future evaluations of subsequent measurements, the camera will be calibrated more accurately in a later stage of development. The results at the physical level are shown in Figure 43.

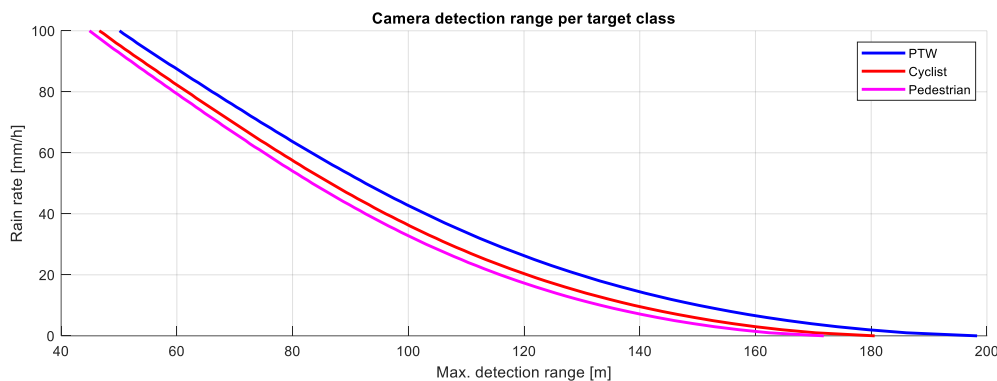


Figure 43: Detection thresholds per target class for camera under rain

Figure 44 shows the detection ranges for different fog visibility for the assumption that visibility in fog equals the maximum detection range.



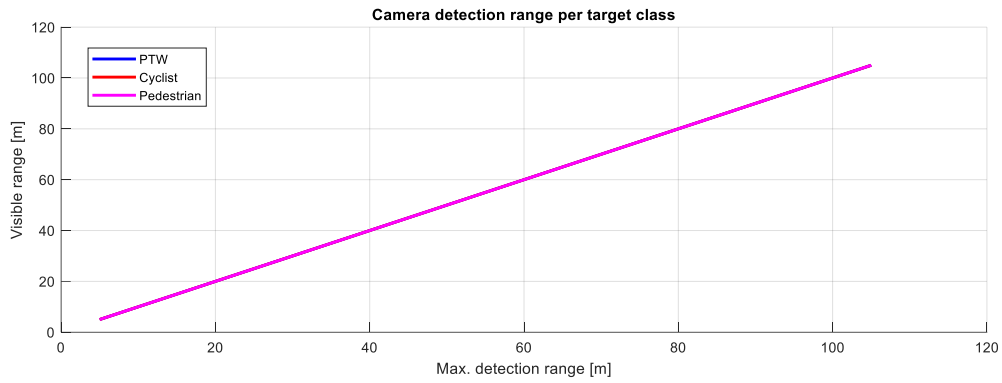


Figure 44: Detection thresholds per target class for camera under fog

The latest version as well as preliminary implementations of the weather filter have been applied and tested successfully in the developed software framework within SAFE-UP. An impression of the virtual weather influence on AVs can be found in a test scenario in the Deliverable report D2.10 (SAFE-UP, Deliverable report D2.10, 2022).



5. Discussion, conclusions and next steps

The results of all investigated measurement campaigns allow a quantification of the adverse weather influence on the different sensor types. The weather effect impacts the sensors' performance, and the different characteristics of the sensors are noticeable. With the quantification of the dominant effects of various weather conditions on different sensor modalities the effects of adverse weather will be integrated into several models for further simulations and analysis (e.g. Deliverable D3.6 of the SAFE-UP project).

During the measurement campaigns performed also the limitations for performing tests with both dynamic testing vehicles and dynamic objects within the test hall became apparent. Therefore a vehicle mounted sensor set was composed and evaluated that will allow the quantification of environmental conditions during measurement and test campaigns in arbitrary locations. Measurement campaigns performed with vehicles equipped with the respective sensor set will provide the possibility of assessing wider ranges of dynamic scenarios, however at the cost of relying quantifiable but uncontrollable environmental conditions.

Development of the weather filter has been finalized. The weather filter is based on a hybrid approach: The physical weather effects on the dampening are analytically calculated, and secondary effects are modelled phenomenologically. The phenomenological modelling is realized by parameterizing the weather filter with the measurement data. The weather filter has also been integrated into the autonomous vehicle model and handed over to SAFE-UP work package 5.



References

ASPECSS. (2014). *Deliverable report D1.7*.

Bijelic, M. G. (2020). Seeing Through Fog Without Seeing Fog: Deep Multimodal Sensor Fusion in Unseen Adverse Weather. *The IEEE/CVF Conference on Computer Vision and Pattern Recognition (CVPR) 2020*.

Campbell Scientific. (2022, September 7th). Retrieved from <https://www.campbellsci.de/cs125>

Robert Bosch GmbH. (2022). Bosch RADAR performance data. *non-public*.

SAFE-UP. (2021). *Deliverable report D2.6*. Deliverable report.

SAFE-UP. (2021). *Deliverable report D3.1*. Deliverable report.

SAFE-UP. (2021). *Deliverable report D3.2*. Deliverable report.

SAFE-UP. (2022). *Deliverable report D2.10*. Deliverable report.

SAFE-UP. (2022). *Deliverable report D3.9*. Deliverable report.

SICK. (2022, September 7th). Retrieved from <https://www.sick.com/de/de/verkehrssensoren/sichtweitemessgeraete/visic620/c/g57494>

Universität Ulm. (2022, September 7th). Retrieved from <https://www.uni-ulm.de/in/iui-drive-u/projekte/dense-datasets/>

Vaisala. (2022, September 7th). Retrieved from <https://www.vaisala.com/en/products/weather-environmental-sensors/mobile-detector-md30>

Waymo. (2022, September 7th). Retrieved from <https://blog.waymo.com/2021/11/a-fog-blog.html>

